

Research Paper

Effects of injection timing and rotational speed on mixture formation and combustion characteristics in a hydrogen/ammonia dual direct injection rotary engine

Weng Fu ^a, Jianfeng Pan ^{a,*}, Baowei Fan ^a, Yi Zhang ^a, Xia Shao ^a, Muhammad Nauman ^a, Wenming Yang ^b

^a School of Energy and Power Engineering, Jiangsu University, Zhenjiang 212013 Jiangsu, PR China

^b Department of Mechanical Engineering, National University of Singapore, 119260, Singapore



ARTICLE INFO

Keywords:

Hydrogen/ammonia
Rotary engine
Direct injection
Injection time
Rotating speed
Combustion characteristics

ABSTRACT

This study investigates the effects of fuel direct-injection (DI) strategies and rotating speed on mixture formation, combustion characteristics, and nitrogen oxides (NOx) formation characteristics using a three-dimensional numerical model. The accuracy of the numerical model is validated through experimental verification. The results demonstrated that hydrogen and ammonia achieved peak cylinder pressures of 3.16 MPa when their direct in-cylinder injection timings were optimized at 250–220 °CA before top dead center (BTDC) and 280–250 °CA BTDC, respectively. This configuration resulted in a maximum increase of 10.10 % in cylinder pressure and a reduction of 10.01 % in combustion duration, compared with C-280-220. Through the formation of gradient mixtures and thermodynamic stratification effects, both strategies-hydrogen-ammonia injection at 250–280 °CA BTDC (Strategy A) and hydrogen-ammonia injection at 220–250 °CA BTDC (Strategy B) demonstrated enhanced combustion efficiency with concurrent mitigation of energy loss. Optimized delayed injection of hydrogen and ammonia reduces NOx emissions by 71.48 %, compared with A-280-280. When the hydrogen injection timing is 220° CA BTDC and the ammonia injection timing is 250° CA BTDC, the optimized rotational speed results in an increase of 11.50 %, 72.21 %, and 26.41 % in cylinder pressure, heat release rate, and effective work, respectively, while reducing NOx emissions by 17.57 %. This study confirms that the coordinated injection phase control of dual fuels, matched with medium and low-speed operating conditions, is an effective approach to achieving efficient and clean combustion in rotary engines.

1. Introduction

In order to address the global energy crisis and promote international cooperation for sustainable development, the Paris Agreement mandates the achievement of net-zero emissions by the middle of the 21st century. In addition to providing strategic guidance for global green and low-carbon development, it also impacts the construction of a shared future for a community [1–3]. Establishing a clean, low-carbon, safe, and efficient energy system represents the cornerstone for realizing this objective. Against this backdrop, power machinery utilizing conventional hydrocarbon fuels, including reciprocating engines and rotary engines, faces significant challenges [4–6]. Compared with traditional reciprocating engines, the Wankel rotary engine (WRE) exhibits distinctive advantages such as compact structure, reduced noise levels,

and superior power-to-weight ratios [7–9]. These merits have facilitated broader applications of WREs in hybrid electric vehicles and unmanned aerial vehicles (UAVs) propulsion systems [10–13], positioning this technology as a current research hotspot.

However, the pursuit of “zero-carbon fuels” is critical for achieving sustainable development in engine technologies. Driven by this imperative, hydrogen [14], ammonia [15], bio-methanol [16], and bio-ethanol [17] have attracted significant attention as promising candidates. Among these zero-carbon alternatives, ammonia stands out as a fully carbon-free clean fuel with mature synthesis processes, cost-effectiveness, and 1.5 times higher hydrogen content per unit volume compared to liquid hydrogen, making it an effective hydrogen energy carrier [18]. These advantages have motivated experimental implementations of ammonia in reciprocating engines [19]. Nevertheless, ammonia combustion faces inherent challenges, including difficult

* Corresponding author at: School of Energy and Power Engineering, Jiangsu University, 301 Xuefu Road, Zhenjiang 212013, PR China.
E-mail address: mike@ujs.edu.cn (J. Pan).

Nomenclature			
ATDC	After the top dead center	PIV	Particle image velocimetry
BTDC	Before the top dead center	SIEF	Sequential ignition and energy feedback
CA10	Crank angle corresponding to 10 % of the in-cylinder fuel heat release	SAGE	Statistical adjoint-gas expansion
CA50	Crank angle corresponding to 50 % of the in-cylinder fuel heat release	UAV	Unmanned aerial vehicles
CA90	Crank angle corresponding to 90 % of the in-cylinder fuel heat release	AMR	Adaptive mesh refinement
CFD	Computational fluid dynamics	CA	Crank angle
ESRM	Energy substitution ratio of methanol	DI	Direct injection
FOC	Front of cylinder	ECU	Electronic control unit
HIA	Hydrogen injection angle	HIT	Hydrogen injection timing
IMEP	Indicated mean effective pressure	IT	Ignition timing
N ₂ O	Nitrous oxide	MOC	Middle of cylinder
OERD	Optimized equivalence ratio distribution	NO ₂	Nitrogen dioxide
		NOx	Nitrogen oxides
		RPA	Radical pool amplification
		SOID:	Start of injection of diesel
		TDC	The top dead center
		λ	Equivalence ratio

ignition and low flame propagation speed, significantly limiting its standalone application in conventional engines [20].

Current research primarily focuses on blending ammonia with high-reactivity fuels to enhance its combustion performance. For instance, Lu et al. [21] investigated ammonia/n-heptane blends in reciprocating engines, identifying distinct low-temperature reactivity characteristics and increased ignition delay times with higher NH₃ mass fractions. Liu et al. [22] conducted numerical simulations on ammonia adaptability in two-stroke engines, demonstrating that diesel pilot ignition enables reliable ammonia combustion. Ryu et al. [23] experimentally studied direct ammonia injection in ammonia/gasoline dual-fuel engines, reporting enhanced volumetric efficiency through direct injection and stabilized combustion via port-injected gasoline. Park et al. [24] characterized ammonia/natural gas combustion in spark-ignition engines, observing substantial CO₂ reduction but compromised combustion efficiency. Mørch et al. [25] validated hydrogen/ammonia blends in reciprocating engines, confirming hydrogen's effectiveness in improving ammonia ignition stability. Based on these studies, it has been demonstrated that the use of ammonia with high-reactivity fuels such as diesel, gasoline, n-heptane, natural gas, or hydrogen [26] can significantly increase its applicability to reciprocating engines.

While the aforementioned studies have advanced our understanding of ammonia/hydrogen combustion in reciprocating engines, rotary engines exhibit distinct characteristics that necessitate targeted investigation. Unlike reciprocating engines, which operate with intermittent combustion cycles and short fuel residence times, rotary engines feature a longer fuel residence time in the combustion chamber due to their eccentric rotor design. This extended duration allows more thorough mixing of gaseous fuels like hydrogen and ammonia, which is critical for ammonia's slow oxidation kinetics [27,28]. Additionally, the nearly continuous combustion process of rotary engines resulting from sequential expansion of three combustion chambers provides a more stable environment for igniting low-reactivity fuels like ammonia, avoiding the cyclic ignition instability common in reciprocating engines [29]. These features make rotary engines inherently more suitable for gaseous fuel blends, where consistent mixing and flame propagation are paramount. However, rotary engines also face unique challenges that influence fuel stratification and combustion. A key issue is apex seal leakage, where gaps between the rotor apex seals and housing allow unburned fuel to escape from the combustion chamber [9]. This leakage disrupts local mixture concentrations, dilutes fuel stratification, and can lead to uneven combustion effects not encountered in reciprocating engines with piston-cylinder seals [30,31]. Addressing how apex seal leakage interacts with hydrogen/ammonia injection strategies is therefore critical for maximizing combustion efficiency in rotary engines, a

gap not covered by reciprocating engine studies.

Building upon these reciprocating engine experiences, selecting appropriate high-reactivity fuels becomes essential for achieving stable ammonia combustion in rotary engines. Nauman et al. [32] have demonstrated that hydrogen is another fully carbon-free renewable fuel that features excellent combustion characteristics, such as a low ignition energy, a wide flammability range, and a rapid flame propagation. Additionally, the rotary engine's unique structural configuration and operation principles make it particularly suitable for the combustion of gaseous fuels [33]. Consequently, the ammonia-hydrogen dual-fuel combination is an ideal alternative for rotary engines [34].

Although port injection has been implemented in single-fuel or conventional dual-fuel engines [35,36], it fails to meet the synergistic combustion requirements of hydrogen/ammonia dual fuels in rotary engines. Kang et al. [37,38] conducted experimental studies on the injection modes of a single-cylinder engine, and the results indicated that compared with the direct injection combined with intake port injection mode, the dual-fuel dual direct injection mode exhibits significant advantages: first, it can generate a higher maximum pressure, thereby achieving high volumetric efficiency and a relatively short combustion duration; second, it has better fuel conversion efficiency; third, the dual direct injection system can significantly expand the engine load. Secondly, due to the continuous rotation of the rotor in rotary engines, the mixing time of hydrogen/ammonia and air is shorter, and port injection tends to cause premature diffusion of hydrogen and ammonia [39]. In particular, hydrogen, due to its high diffusivity, will be excessively diluted, resulting in the loss of the ability to stabilize flames and ignite low-reactivity ammonia. Finally, through independent injection control, dual direct injection can form a favorable distribution of the mixture, counteract the impact of apex seal leakage, ensure sufficient fuel concentration in key ignition zones, and improve combustion efficiency.

Current literature on engine direct injection strategies demonstrates that fuel-air mixture distribution in flow fields critically influences combustion characteristics. For instance, Rameez et al. [40] systematically investigated hydrogen-diesel dual-fuel combustion, focusing on pulse distribution ratios and first-pulse injection timing variations. Their experimental study revealed that progressively advancing injection timing substantially reduced NOx emissions without compromising performance parameters. Yang et al. [41] experimentally explored the synergistic effects of methanol energy substitution ratio (ESRM) and diesel injection timing (SOI_D) in methanol-diesel dual direct-injection engines. The results indicated that ESRM and SOI_D significantly modulate combustion phasing and emission profiles, with optimized coordination demonstrating potential for enhanced engine performance. Wang et al. [42] investigated the impacts of injector angle and multi-

injection strategies on ammonia-diesel dual-fuel combustion. They found that reducing the injector angle effectively reduced NOx emissions, as well as marginally reducing thermal efficiency. In another study, Wang et al. [43] experimentally analyzed diesel-natural gas dual-fuel injection strategies, identifying that peak in-cylinder pressure was predominantly governed by natural gas injection timing, with injection phasing exerting critical control over combustion progression. Feng et al. [44] developed a three-dimensional computational model for diesel-methanol dual direct-injection engines, examining how nozzle geometry parameters including diameter (D), inlet radius (R), and length (L) affect internal fuel flow and combustion dynamics. Experimental validation further demonstrated that nozzles with $D = 1.65$ mm achieved optimal combustion temperatures and pollutant emission profiles. Fan et al. [45] numerically investigated hydrogen injection timing (HIT) and hydrogen injection angle (HIA) on mixture formation, flame propagation, and NO emissions. Their results revealed that HIT and HIA significantly altered flame propagation pathways by modifying fuel stratification patterns, thereby improving combustion efficiency.

In summary, existing studies have mostly focused on the combustion characteristics of ammonia blended with high-reactivity fuels in reciprocating engines, with insufficient attention paid to the mixture formation and combustion characteristics of hydrogen/ammonia dual direct injection in rotary engines. There is also a lack of exploration into the coupling effects between injection strategies and rotational speeds, along with inadequate consideration of the impact of the unique structures of rotary engines (such as eccentric design, continuous combustion mode, and apex seal leakage) on combustion. Additionally, traditional injection methods struggle to meet the requirements for synergistic combustion of dual fuels in such engines. This study, through three-dimensional numerical simulation combined with experimental verification, targets hydrogen/ammonia dual direct injection rotary engines, coordinately regulates the injection timings of the two fuels and rotational speeds, and reveals the laws governing mixture formation, combustion characteristics, and nitrogen oxide generation, thereby providing theoretical support for achieving efficient and clean combustion in rotary engines.

2. Establishment and verification of mathematical model

2.1. Geometric model and grid generation

The established 2D and 3D models of the dual direct-injection Hydrogen-Ammonia rotary engine (HARE) are illustrated in Fig. 1(a) and Fig. 1(b). Constructed based on parametric functions in CREO, the model incorporates detailed engine parameters listed in Table 1. The rotary engine structure comprises eight functional domains: intake port, exhaust port, three combustion chambers, hydrogen injector, ammonia injector, and spark plug. The ammonia injector is integrated into the main shaft of the rotor housing, while the hydrogen injector is positioned 30 mm above the main shaft. Both gaseous injectors employ a nozzle diameter of 2 mm. The 3D model was imported into CONVERGE CFD software, which features a unique adaptive mesh refinement (AMR) capability to enhance computational accuracy.

As shown in Fig. 2, the base grid size was set to 4 mm, with the intake port assigned a refinement level of 0. The combustion chambers were discretized at refinement level 1 (2 mm grid). To resolve ignition dynamics, a spherical ignition zone with a 2 mm radius was defined near the spark plug. Cylindrical refinement zones (level 4, 0.25 mm grid) were implemented around the spark plug and injectors. AMR was activated across all domains, with gradient-based triggers for temperature (20 K), velocity (5 m/s) and mixture concentration (0.1) thresholds, constrained to refinement level 3 (0.5 mm grid). This meshing strategy has been validated to meet computational accuracy requirements in prior studies [22].

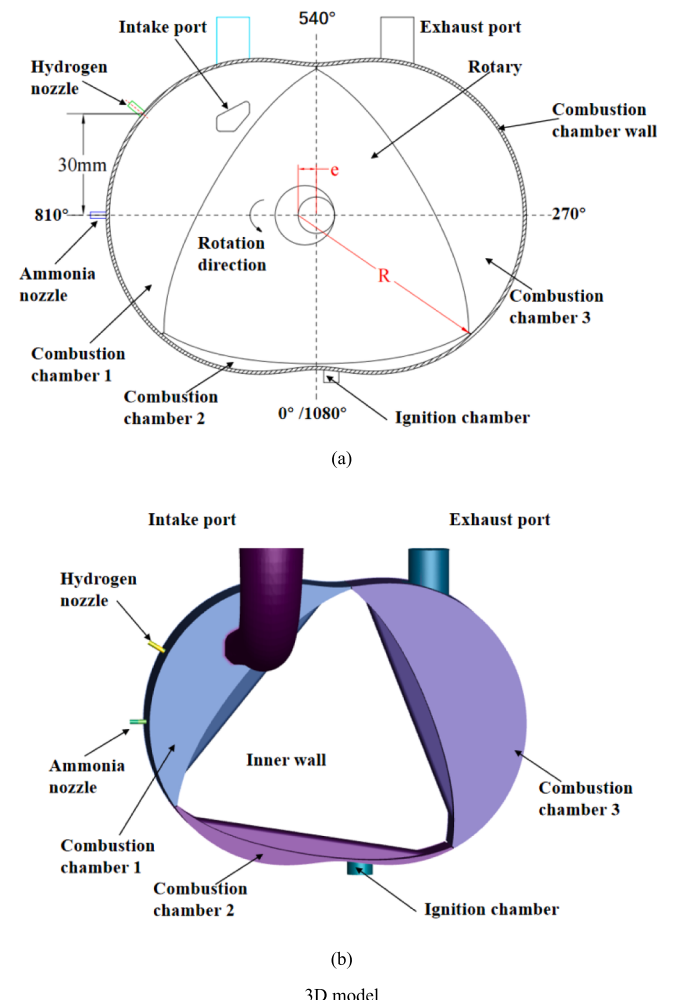


Fig. 1. Geometric model of the rotor engine.

Table 1
Major parameters of Z160F gasoline rotary engine [27].

Engine parameters	Value
Number of rotors	1
Cooling mode	Air cooling
Ignition type	Spark plug ignition
Displacement	160000 mm ³
Compression ratio	8
Generating radius	69 mm
Eccentricity	11 mm
Chamber width	40 mm
Intake timing	615 °CA(BTDC), 207 °CA(BTDC)
Exhaust timing	208 °CA(ATDC), 610 °CA(ATDC)

2.2. Selection and validation of turbulence model

Regarding the turbulence model, the RNG k- ϵ turbulence model is highly suitable for calculating vortex variations in rotary engines [46]. Therefore, this study also employs this model. To validate the reliability of the RNG k- ϵ [47,48] turbulence model, in our previous work, we used Particle Image Velocimetry (PIV) to capture the flow field at the cylinder center section of an optical rotary engine and obtained the flow field calculated using the RNG k- ϵ model under PIV experimental conditions. Additionally, the flow field at the cylinder center was calculated using the RNG k- ϵ turbulence model at 700 rpm. A comparison of the PIV test results and the calculated results is shown in Table 2. As can be seen from Table 2, the RNG k- ϵ model fits the experimental flow field well

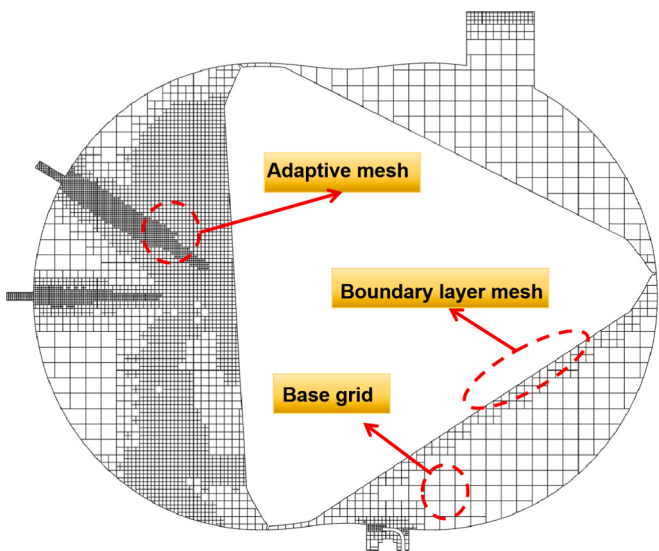


Fig. 2. The grid diagram of the hydrogen/ammonia rotary engine.

[49].

2.3. Selection and validation of combustion model

Combustion models are classified into premixed and non-premixed combustion models, including various models such as SAGE, CTC/Shell, and CEQ. Among them, the SAGE combustion model offers high flexibility, allowing for the incorporation of detailed chemical reaction mechanisms for various components, which significantly improves the accuracy of cylinder combustion process simulations. Therefore, this study selects the SAGE combustion model for numerical simulations of the in-cylinder combustion process. When simulating the combustion process of the rotary engine, an appropriate chemical reaction kinetics model must also be selected to accurately simulate the concentration changes of key components and the flame propagation dynamics within the cylinder during the combustion process. In addition, when selecting the chemical reaction mechanism, computational accuracy, cycle efficiency and economic cost must be considered. Therefore, to balance computational accuracy with time cost and efficiency, this study chooses the SAGE combustion model coupled with the simplified reaction mechanism proposed by Gabriel J. Gotama et al [50], which includes 26 components and 119 chemical reactions. This mechanism can effectively predict the flame combustion velocity over a wide range of equivalence ratios. This mechanism is more suitable for hydrogen/ammonia dual-fuel combustion in rotary engines. Unlike general mechanisms, the development of this model focuses on low-carbon fuel blends, specifically capturing the key reaction pathways of ammonia oxidation and hydrogen-assisted combustion, which are the core of the combustion dynamics in our research. Equally importantly, our experimental and simulation results demonstrate a high-precision match when using this mechanism.

The accuracy of the combustion model in numerical simulations needs to be validated by experimental data. In the experiments, when the equivalence ratio was 0.8, we conducted tests on a rotary engine fueled with ammonia/hydrogen under various speed conditions and collected data, including in-cylinder pressure. This study is based on the Z160F model single-spark gasoline rotary engine, with specific parameters listed in Table 1. For the original test engine, we first fabricated corrosion-resistant intake ducts and ammonia-specific injectors and installed an exhaust system and an emissions treatment device. A schematic diagram of the experimental setup is shown in Fig. 3. The professional instrument list and errors of used in the experiment is displayed in Table 3. The in-cylinder pressure and torque variations caused

by the working mixture can be measured using a cylinder pressure sensor and a torque sensor. The dynamometer can adjust parameters such as rotating speed, the ECU system can adjust intake and ignition parameters, and the combustion analyzer system can record real-time changes in the air-fuel ratio during the combustion process.

In terms of numerical simulation, we built a simulation model in CONVERGE software, set the initial and boundary conditions, and incorporated the SAGE combustion model for accurate combustion process simulation. Then, we assessed the credibility of the combustion model by comparing the experimental measurement data with the simulation results. The comparison of in-cylinder pressure is shown in Fig. 4. It can be observed that the actual test results are in high agreement with the numerical simulation predictions using the SAGE combustion model [49,51], with the comparison error for in-cylinder pressure controlled within 7.14 % [52].

3. Development of a calculation methodology

Fuel injection timing serves as a critical determinant in engine research, directly governing performance metrics, thermodynamic efficiency, and emission characteristics. Optimal injection phasing facilitates enhanced air-fuel mixing homogeneity, thereby improving combustion efficiency and suppressing NOx emissions. Premature injection timing risks inducing knocking phenomena, while delayed timing triggers incomplete combustion and power output reduction. Precision control of injection timing enables combustion process optimization, strengthening operational reliability and component longevity. Furthermore, injection timing requirements vary significantly across different operational conditions, necessitating systematic investigation and calibration to maintain optimal performance across diverse operating regimes.

This study focuses on the Z160F Wankel rotary engine to investigate optimal injection strategies for hydrogen/ammonia dual direct injection (DI), with the numerical simulation protocol detailed in Table 4. The injection pressure of hydrogen was 3.5 bar, and that of ammonia was 2.5 bar, with the ignition timing set at 40 °CA (BTDC). The injection duration of hydrogen and ammonia is 30 °CA. For operational case identification, simulation schemes are labeled as [Case identifier]-[Hydrogen injection timing]-[Ammonia injection timing]. For instance, Case A-340-280 denotes hydrogen injection at 340° CA before top dead center (BTDC) and ammonia injection at 280° CA BTDC, with analogous nomenclature applied to other test conditions.

4. Results and discussion

4.1. Hydrogen-Ammonia injection timing on rotary engine combustion & emissions

4.1.1. Combustion characteristics: Cylinder pressure and duration

The injection timing in hydrogen-ammonia rotary engines significantly influences engine performance. Appropriate injection timing ensures the thorough mixing of hydrogen ammonia with air, precisely determines combustion initiation, maintains stable combustion rates, and achieves smooth and efficient combustion.

Fig. 5 illustrates the effects of different hydrogen/ammonia injection timings on in-cylinder pressure in the rotary engine, where Fig. 5(a)-(e) correspond to the cylinder pressure curves of Case A to Case E, respectively. Overall, varying injection timings for H₂ and NH₃ induce similar trends in in-cylinder pressure evolution. The pressure variation is consistent with the theory of turbulent flame propagation, where injection timing governs the initial fuel-air distribution that subsequently determines flame front development [53]. While varying injection timings for H₂ and NH₃ induce similar pressure evolution trends, the differential molecular diffusion rates between hydrogen (0.61 cm²/s) and ammonia (0.25 cm²/s) create distinct stratification patterns.

This study primarily focuses on the analysis of Fig. 5(a). As shown in

Table 2

Comparison of PIV experimental results and simulation calculation results at 700 RPM [49].

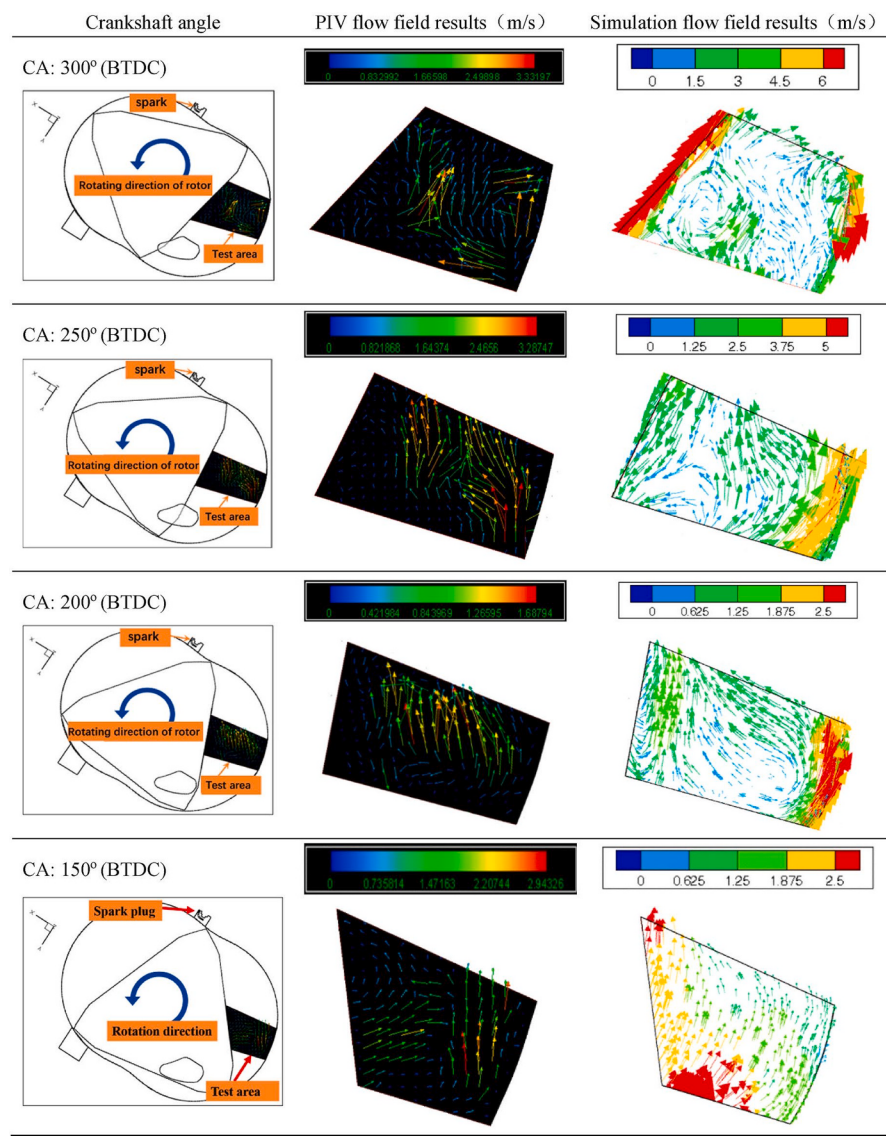


Fig. 5(a), when ammonia injection is initiated at 280 °CA BTDC, peak cylinder pressure exhibits a pronounced “valley-peak” trajectory across H₂ injection timings: the peak in-cylinder pressures corresponding to hydrogen injection timings of 340 °CA BTDC, 310 °CA BTDC, 280 °CA BTDC, 250 °CA BTDC, and 220 °CA BTDC are 2.26 MPa, 2.27 MPa, 1.94 MPa, 3.16 MPa, and 2.38 MPa, respectively. This trajectory indicates that concurrent injection of H₂ and NH₃ (280 °CA BTDC) induces sub-optimal combustion, while a 30 °CA delay in H₂ injection (250 °CA BTDC) yields the highest pressure development. Notably, the A-250-280 case demonstrates a 10.10 % increase in peak cylinder pressure compared to the C-280-220 configuration. This enhancement is attributed to variations in fuel injection timing, which alter the spatial distribution of hydrogen and ammonia within the combustion chamber, thereby affecting mixture formation characteristics. These phenomena arise from the coupling of fuel stratification patterns, turbulent mixing dynamics, and flame propagation kinetics, as validated by in-cylinder flow field and species distribution data (Figs. 8 and 9).

As illustrated in Fig. 5 (f), when hydrogen injection timing is fixed at 250 °CA, the variations in peak pressure and corresponding crank angle positions with different ammonia injection timings reveal that higher in-

cylinder pressures correlate with advanced peak pressure phasing. This phenomenon is primarily attributed to the homogeneous distribution of hydrogen and ammonia mixtures, which promotes accelerated combustion rates and consequently reduces the combustion duration. Among the tested NH₃ injection timings, the configurations at 280 °CA BTDC and 250 °CA BTDC demonstrate maximum peak pressures of 3.17 MPa and 3.15 MPa, respectively. These peak pressures occur at 1090.81 °CA and 1094.92 °CA, indicating a phase advancement of 4.11 °CA between the two optimal injection timings.

The trends in Fig. 5 underscore that coordinated retarding of H₂ (250 °CA BTDC) and NH₃ (250–80 °CA BTDC) injection optimizes mixture stratification by leveraging their differential reactivity and diffusion properties. This strategy resolves the trade-off between ignition propensity (via localized H₂ enrichment) and combustion completeness (via homogenized NH₃), yielding enhanced pressure development.

In addition, the consumption rate curves of hydrogen and ammonia are shown in Fig. 6 (a) and 6(b). As can be seen from the figure, both fuels are completely consumed at the end of the combustion process, with the consumption rate reaching 100 %. This result indicates that under the operating conditions investigated in this study, the residual

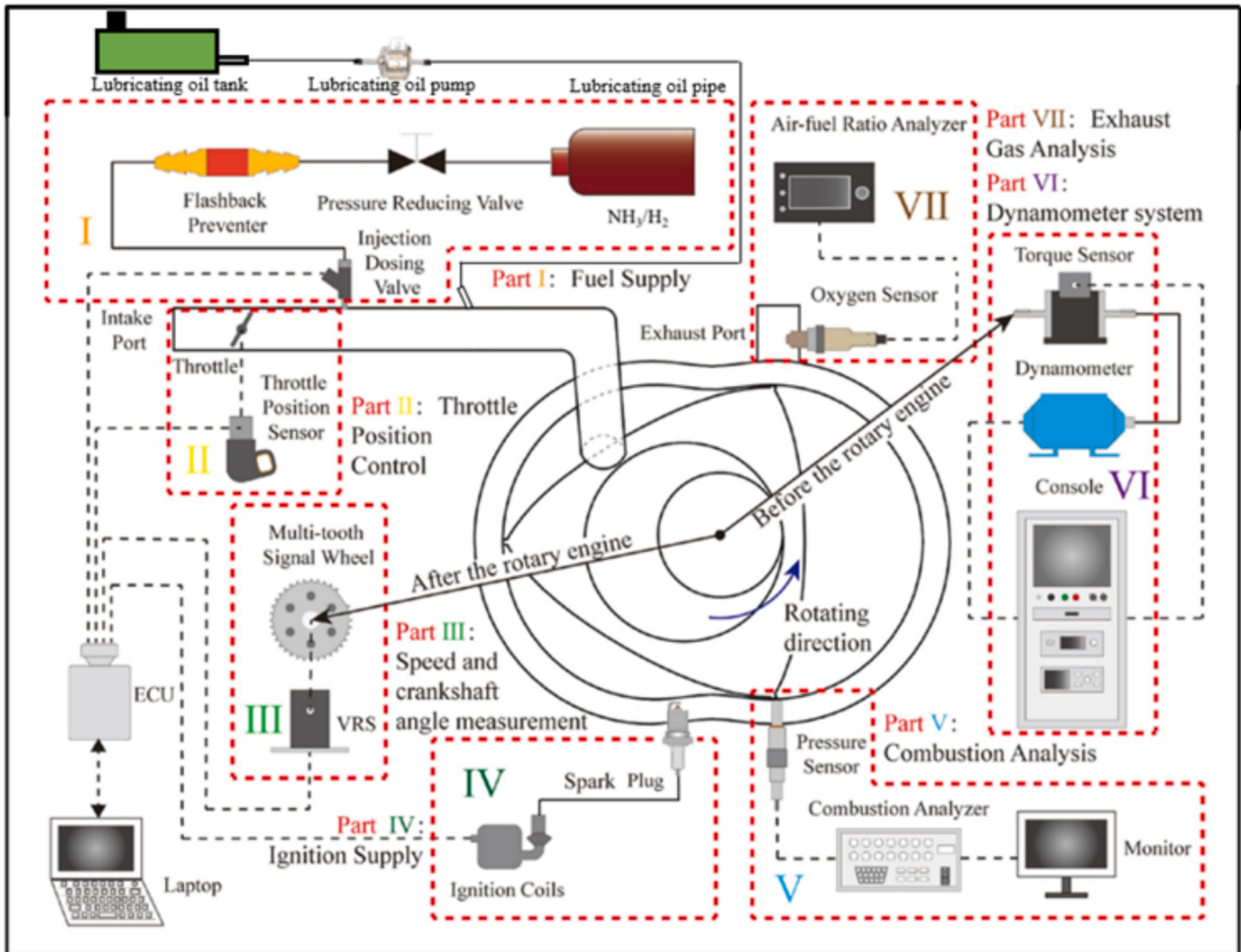


Fig. 3. Schematic diagram of the experimental setup for ammonia/hydrogen rotary engine.

Table 3
Professional instrument list and experimental errors.

Parameter	Manufacturer	Type	Uncertainty
Engine speed	Shenma	YVP132M-4	$\pm 0.1\%$
Torque	Polytronics	JH-50	$\pm 0.1\%$
Flow rate	Changcheng	ALM-LED	$\leq 0.2\%$
Air-to-fuel ratio	ECOEFI	HZB2000	± 0.008
In-cylinder pressure	KISTLER	6125C	$<\pm 0.3\text{ bar}$

amount of unburned ammonia is negligible, confirming that clean combustion and low-emission green operation modes can be achieved within the rotary engine.

Fig. 7 illustrates the effects of different hydrogen/ammonia injection timings on ignition delay, CA50, and combustion duration. As demonstrated in Fig. 7(a)–(c), in-cylinder direct injection timing of hydrogen/ammonia significantly influences CA10, CA50, and combustion duration. Particularly, configurations A-250-280 and B-220-250 exhibited the shortest CA10, CA50, and combustion duration among all tested hydrogen/ammonia timing combinations, achieving reductions of 50.30 %, 38.39 %, 7.16 %, 7.54 %, and 10.01 %, 6.12 % respectively, compared to C-280-220. These optimized combustion parameters align with the maximum peak cylinder pressures observed in Fig. 5(a) and Fig. 5(b).

Analysis of Fig. 7(a) reveals a non-monotonic trend in ignition delay

when hydrogen injection timing is fixed at 220 °CA BTDC: the ignition delay initially decreases, then increases with retarded ammonia injection timing. This phenomenon is attributed to reduced fuel residence time in the combustion chamber at moderately delayed injection timings, which forces accelerated combustion completion within a constrained time frame. However, excessive injection retard deteriorates combustion efficiency due to compromised ammonia distribution homogeneity, ultimately prolonging the ignition delay period.

4.1.2. The influence of in-cylinder mixture formation

To investigate the effects of hydrogen and ammonia direct injection on in-cylinder flow dynamics, four representative operating conditions (A-250-280, A-280-280, B-220-250, and B-340-250) were selected for comparative analysis of flow field characteristics and hydrogen/ammonia distribution patterns.

Fig. 8 delineates the hydrogen distribution and flow field evolution under varying crank angles for different hydrogen/ammonia direct injection strategies. Comparative analysis of hydrogen distribution relative to ignition timing reveals distinct stratification across four operating conditions. Before ignition, conditions A-250-280 and B-220-250 exhibit pronounced hydrogen stratification, with fuel concentrated in the Front of cylinder (FOC) and Middle of cylinder (MOC) regions. In contrast, Conditions B-340-250 and A-280-280 demonstrate progressively reduced stratification, achieving uniform hydrogen distribution across FOC, MOC, and Back of cylinder (BOC) zones. Detailed examination of

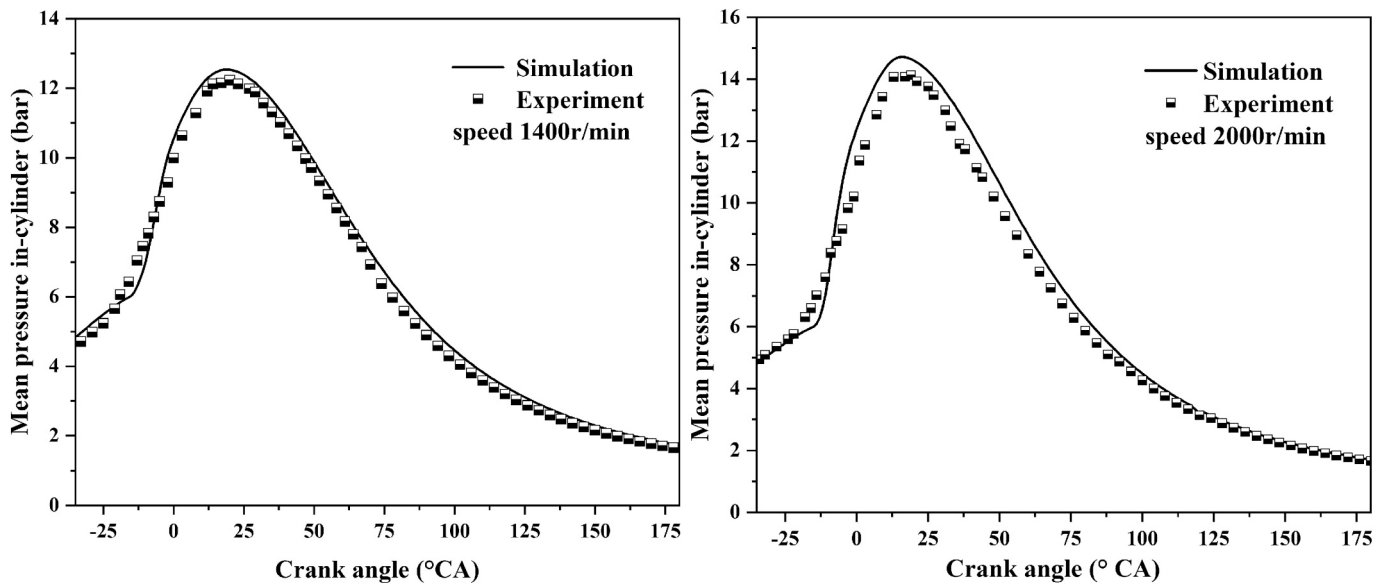


Fig. 4. Comparison of experimental and simulated in-cylinder pressures of ammonia/hydrogen rotary engine with different speeds.

Cases A-250-280 and A-280-280 highlights injection timing effects on vortex-driven dispersion. At 15 °CA post-injection, delayed hydrogen injection in A-250-280 generates large-scale vortices (Vortex A and Vortex B), facilitating hydrogen transport to FOC and BOC. Conversely, A-280-280 develops smaller vortices that preferentially direct hydrogen toward BOC. By 45 °CA post-injection, A-250-280 manifests a dominant FOC vortex with high hydrogen concentrations near chamber walls.

Wall-jet interactions at 80 °CA before the top dead center (TDC) establish distinct stratification layers in this case. In A-280-280, hydrogen remains concentrated near BOC/FOC walls but exhibits diminished concentration gradients, attaining homogeneous distribution by 80 °CA BTDC due to attenuated vortex influence. Vortex breakdown near TDC in both conditions arises from unidirectional flow patterns inherent to rotary engine architectures. Post-ignition analysis shows A-250-280 maintains hydrogen concentration primarily in FOC/MOC zones, while A-280-280 achieves a 25.24 % reduction in global hydrogen concentration with enhanced full-chamber dispersion. Notably, hydrogen distribution patterns in A-280-250 and B-340-250 exhibit structural similarities. The B-220-250 condition demonstrates complete hydrogen confinement to FOC/MOC regions (BOC concentration = 0), a configuration that optimizes combustion efficiency by restricting fuel localization to high-turbulence zones.

At 25 °CA BTDC, in Conditions A-250-280 and B-220-250, hydrogen remains highly concentrated in the FOC/MOC regions (with zero concentration in the BOC for B-220-250). The combustion-driven flow field exhibits radial expansion, yet the pre-existing stratification structure continues to dictate the distribution pattern. At TDC, rotor compression forces the high-concentration hydrogen in FOC/MOC toward the cylinder walls. By 15 °CA ATDC, hydrogen combustion is nearly complete, especially in B-220-250. Conversely, in Conditions A-280-280 and B-340-250, the hydrogen concentration gradient across the cylinder is significantly reduced at 25 °CA BTDC. The flow field, characterized by weak vortices, maintains uniform mixing, enabling synchronized combustion across all regions. As the rotor rotates, hydrogen in the FOC region is fully consumed.

Fig. 9 illustrates the in-cylinder ammonia distribution and flow field evolution under varying hydrogen/ammonia injection timings. Comparative analysis of ammonia distribution relative to ignition timing reveals distinct stratification patterns: Conditions A-280-280 and B-340-250 exhibit pronounced ammonia stratification concentrated in the FOC and MOC regions, whereas Conditions A-250-280 and B-220-250 demonstrate homogeneous ammonia dispersion throughout the

combustion chamber. At 15 °CA post-ammonia injection, Cases A-250-280 and B-220-250 show fuel accumulation predominantly in the MOC. Subsequent hydrogen injection induces flow reorientation, redistributing ammonia toward FOC and BOC regions by 45 °CA post-injection. Unidirectional flow interactions homogenize ammonia distribution by 80 °CA before TDC, with further uniformity enhancement observed at ignition timing. This configuration facilitates rapid ammonia combustion despite an overall concentration reduction. In contrast, Cases A-280-280 and B-340-250 exhibit initial ammonia accumulation in FOC/MOC at 15 °CA post-injection. Vortex-driven flow patterns redirect ammonia toward FOC/BOC by 45 °CA post-injection, culminating in persistent stratification at ignition timing. This inhomogeneous distribution impedes combustion efficiency due to ammonia's high ignition energy requirement and flame propagation rates of merely 10 % of hydrogen.

At 25 °CA BTDC, in Conditions A-250-280/B-220-250, hydrogen ignites ammonia to break through the ignition barrier, with the MOC already fully combusted. At TDC, rotary engine compression promotes the completion of combustion in the FOC/MOC. By 15 °CA ATDC, ammonia burns sufficiently, and A-250-280 is nearly completely consumed. In contrast, in Conditions A-280-280/B-340-250, ammonia exhibits a stratified distribution with high concentration at 25 °CA BTDC, resulting in slow ignition by hydrogen, with only a portion of the MOC undergoing combustion. At TDC, the combustion efficiency in the FOC and MOC increases. By 15 °CA ATDC, a large amount of ammonia remains in the BOC, possibly due to the temperature failing to reach the ignition threshold, leading to high-concentration accumulation in this region.

These observations align with previous in-cylinder pressure measurements, suggesting that optimal combustion efficiency occurs when hydrogen stratification (FOC/MOC concentration) coexists with homogeneous ammonia distribution. The improved flame speed under hydrogen-core and ammonia-shell stratification arises from three synergistic mechanisms that leverage the distinct combustion properties of H₂ and NH₃ [32]. The first one is the Sequential Ignition and Energy Feedback (SIEF). In this mechanism, H₂, with its high flame and low ignition ignites first in the core region. This rapid initial combustion releases heat immediately, raising the local temperature in the hydrogen core to about 2000–500 K, which exceeds the minimum ignition temperature of ammonia [54]. This thermal feedback lowers the activation energy barrier for ammonia oxidation in the surrounding shell and enables the ammonia to ignite faster than it would in a homogeneous

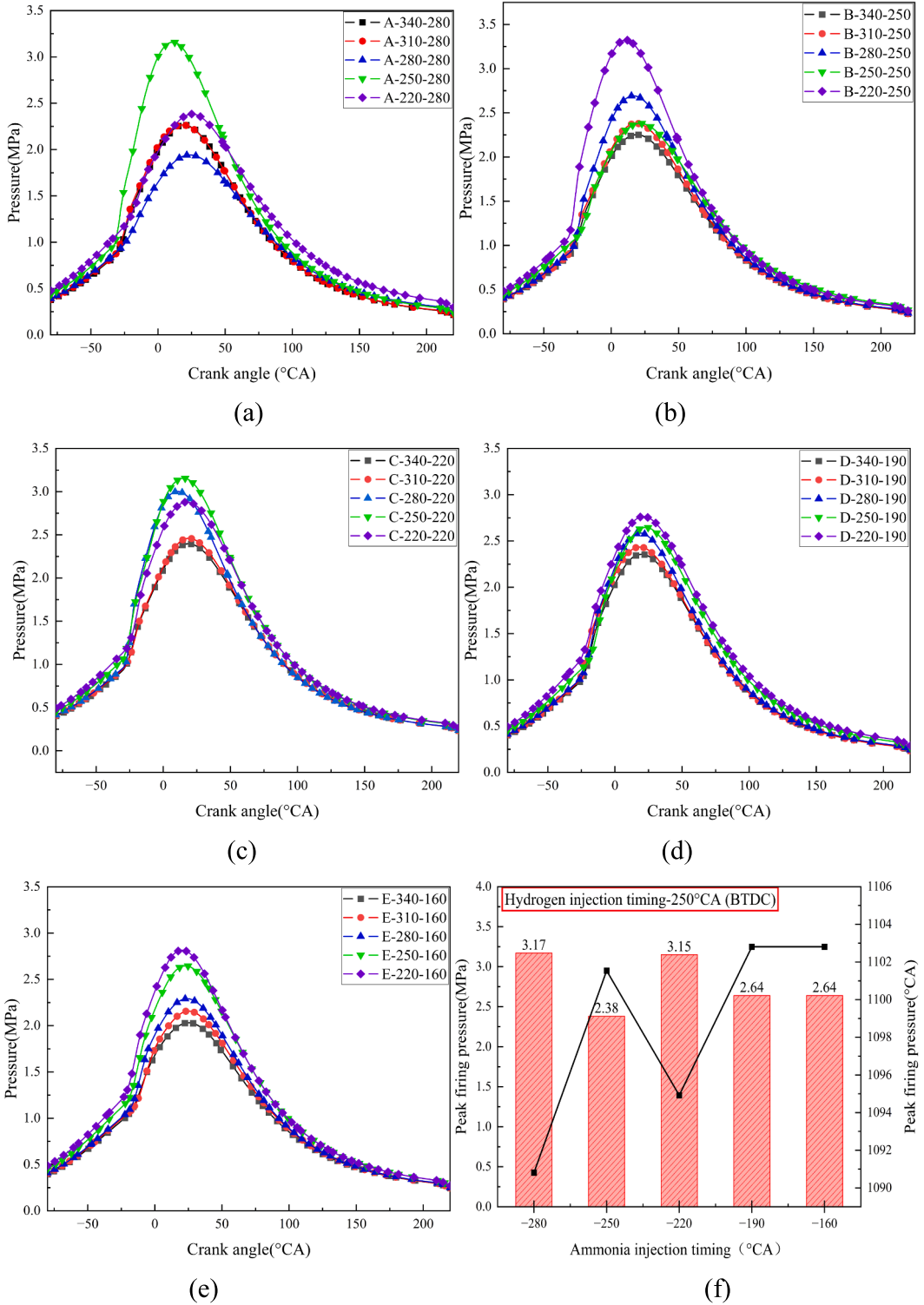
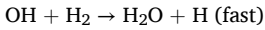
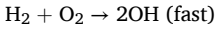


Fig. 5. In-cylinder pressure under different hydrogen/ammonia injection timings.

mixture [33]. The second mechanism is the Radical Pool Amplification (RPA), where H₂ combustion in the core generates a high concentration of reactive radicals like H, OH, and O via chain reactions [50].



These radicals diffuse outward into the ammonia shell, thereby accelerating NH₃ decomposition and oxidation. Ammonia's oxidation

typically requires radical-driven initiation, and the surplus radicals from the hydrogen core bypass the slow radical-formation stage of ammonia's combustion, directly boosting reaction rates in the shell [45]. In the third mechanism called the Optimized Equivalence Ratio Distribution (OERD), the stratification inherently creates a favorable equivalence ratio gradient where i. The hydrogen core operates at a moderately rich ϕ , where hydrogen's flame speed peaks and ii. The ammonia shell, surrounding the core, resides in a lean-to-stoichiometric range where ammonia's flame speed, though lower than hydrogen's, is less inhibited

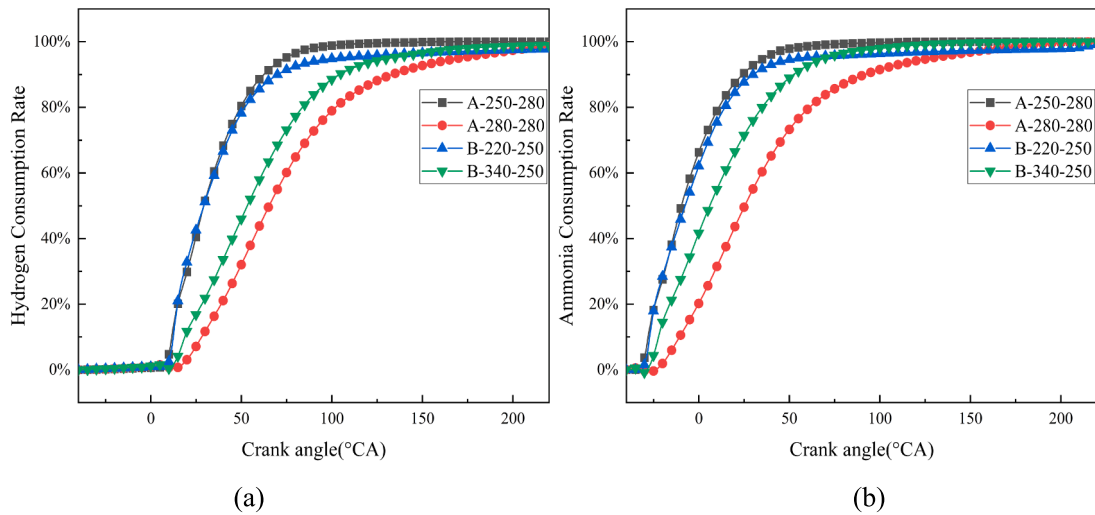


Fig. 6. Consumption rates of hydrogen and ammonia under varied hydrogen/ammonia injection timings.

Table 4
The calculation scheme with different direct injection timing strategies.

Case	H ₂ injection timing (BTDC)	NH ₃ injection timing (BTDC)
A-340-280	340 °CA(BTDC)	280 °CA(BTDC)
A-310-280	310 °CA(BTDC)	280 °CA(BTDC)
A-280-280	280 °CA(BTDC)	280 °CA(BTDC)
A-250-280	250 °CA(BTDC)	280 °CA(BTDC)
A-220-280	220 °CA(BTDC)	280 °CA(BTDC)
B-340-250	340 °CA(BTDC)	250 °CA(BTDC)
B-310-250	310 °CA(BTDC)	250 °CA(BTDC)
B-280-250	280 °CA(BTDC)	250 °CA(BTDC)
B-250-250	250 °CA(BTDC)	250 °CA(BTDC)
B-220-220	220 °CA(BTDC)	250 °CA(BTDC)
C-340-220	340 °CA(BTDC)	220 °CA(BTDC)
C-310-220	310 °CA(BTDC)	220 °CA(BTDC)
C-280-220	280 °CA(BTDC)	220 °CA(BTDC)
C-250-250	250 °CA(BTDC)	220 °CA(BTDC)
C-220-220	220 °CA(BTDC)	220 °CA(BTDC)
D-340-190	340 °CA(BTDC)	190 °CA(BTDC)
D-310-190	310 °CA(BTDC)	190 °CA(BTDC)
D-280-190	280 °CA(BTDC)	190 °CA(BTDC)
D-250-190	250 °CA(BTDC)	190 °CA(BTDC)
D-220-190	220 °CA(BTDC)	190 °CA(BTDC)
E-340-160	340 °CA(BTDC)	160 °CA(BTDC)
E-310-160	310 °CA(BTDC)	160 °CA(BTDC)
E-280-160	280 °CA(BTDC)	160 °CA(BTDC)
E-250-160	250 °CA(BTDC)	160 °CA(BTDC)
E-220-160	220 °CA(BTDC)	160 °CA(BTDC)

by fuel dilution [25]. The hypothesis has been validated by systematically analyzing the temperature fields of the four representative conditions.

In summary, analysis of hydrogen/ammonia distribution patterns under varied injection timings (Case 4 in Conditions A-250-280 and B-220-250, Fig. 8 and Fig. 9) demonstrates that hydrogen-core/ammonia-shell stratification promotes optimal combustion efficiency through enhanced flame front propagation. This dual-fuel configuration facilitates localized hydrogen enrichment at ignition nuclei while maintaining ammonia homogeneity in peripheral zones, achieving a 10.01 % reduction in combustion duration compared to baseline cases. Conversely, inverted configurations with ammonia-rich cores impede complete combustion due to hydrogen's suppressed diffusion toward flame anchoring regions. Notably, the earlier injection timing for ammonia (compared to hydrogen) is strategically chosen to compensate for its slower diffusion rate (0.25 cm²/s vs. 0.61 cm²/s for hydrogen). Ammonia requires extended residence time to fully evaporate and mix uniformly with air, avoiding localized rich zones that hinder

combustion. In contrast, hydrogen's rapid diffusivity allows delayed injection, enabling targeted stratification in FOC/MOC regions to enhance flame propagation a synergistic strategy leveraging each fuel's unique physical properties.

These observations align with the pressure-derived combustion phasing data, confirming that hydrogen-core stratification optimizes thermal efficiency by synchronizing fuel reactivity gradients with turbulent flame development. The vortex-driven transport mechanisms identified in Cases A-250-280/B-220-250 provide critical insights for designing stratified-charge combustion systems in dual-fuel engines.

Fig. 10 delineates the unburned hydrogen distribution within the combustion chamber under varying hydrogen/ammonia injection timings at different crank angles. At 30 °CA BTDC, the high hydrogen concentration near the spark plug is rapidly ignited, initiating instantaneous flame propagation toward peripheral regions. Condition A-280-280 exhibits the minimal combustion zone, with hydrogen depletion confined predominantly to the spark vicinity. Across all configurations, near-complete fuel consumption is observed in the FOC while residual unburned mixtures persist in the BOC. By 15 °CA ATDC, Condition A-250-280 achieves full oxidation of fuel in both FOC and MOC, demonstrating the largest combustion zone among the tested cases. Comparative analysis reveals that combustion inefficiencies primarily correlate with fuel accumulation in BOC, where restricted flame anchoring and delayed oxidation kinetics impede rapid combustion. This spatial fuel distribution gradient results in a 12-15 % reduction in combustion efficiency for BOC-dominant cases, as quantified by heat release rate analysis.

These findings, supported by combustion temperature contours and thermal imaging [49], confirm that optimizing hydrogen stratification in FOC/MOC regions enhances combustion completeness through the synchronization of turbulent flame dynamics with fuel reactivity gradients. The observed flame propagation patterns provide critical insights for refining injection strategies in hydrogen/ammonia rotary engines to mitigate unburned emissions and improve thermal efficiency.

4.1.3. Effect on the temperature field

Fig. 11 shows the temperature profiles under varied hydrogen/ammonia DI timings across crank angles. Analysis reveals a rapid temperature rise during combustion initiation followed by gradual post-ignition decay. The peak in-cylinder mean temperatures for the four conditions rank as follows: A-250-280 > B-220-250 > B-340-250 > A-280-280, correlating with observed peak cylinder pressures and flow field mixture distribution patterns. Delayed hydrogen injection timing enhances in-cylinder temperature, as evidenced by elevated thermal

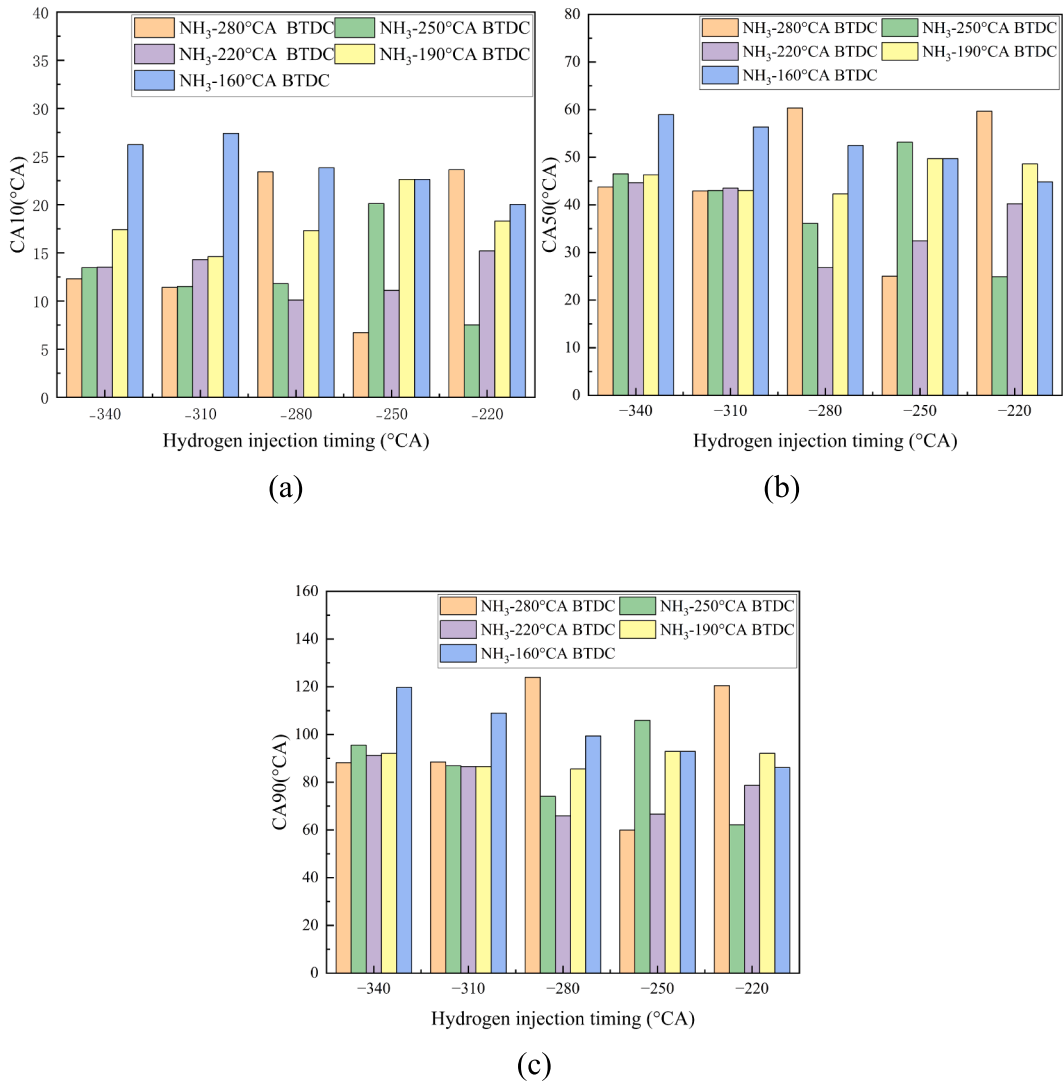


Fig. 7. Ignition delay, CA50 and combustion duration under different Hydrogen/Ammonia injection timings.

conditions at TDC for A-250-280 and B-220-250 in Fig. 12. Furthermore, moderate retardation of ammonia injection timing improves combustion efficiency through temperature elevation.

Fig. 12 illustrates crank angle-resolved temperature contours under different hydrogen/ammonia DI strategies. Among them, A, B, and C in Fig. 12 represent 3D contour, top views, and 2D front views respectively. All conditions exhibit concentrated high-temperature zones in the front and central chamber regions, with residual unburned zones persisting in the rear region. This spatial thermal gradient confirms fuel accumulation in rear chamber zones (BOC), which impedes complete combustion due to suppressed flame propagation.

In summary, flame propagation dynamics are governed by fuel distribution patterns, critically influencing overall combustion efficiency. For hydrogen/ammonia DI strategies, optimal mixture stratification should localize near the spark-adjacent front/central chamber regions to accelerate flame front development. Concurrently, hydrogen accumulation in rear chamber zones (BOC) must be minimized to avoid delayed oxidation during late combustion phases. Comparative data demonstrate that later hydrogen injection timings enhance HARE performance, achieving simultaneous fuel reactivity and turbulent flame interaction.

4.1.4. Effect on emission performance

Fig. 13 illustrates the impact of hydrogen/ammonia dual direct injection timings on emission characteristics. Comparative analysis of

Conditions A-250-280 and A-280-280 demonstrates that delayed hydrogen injection timing effectively reduces NOx emissions, primarily attributed to enhanced combustion completeness in A-250-280, which suppresses thermal NO formation through localized temperature moderation.

When the rotational speed is 1400 r/min, among conditions B-220-250 and B-340-250, B-220-250 exhibits the lowest NO emission (a 71.48 % reduction compared with A-280-280), while the concentrations of nitrous oxide (N₂O) and nitrogen dioxide (NO₂) increase [55]. This phenomenon arises from peak in-cylinder pressures and optimized combustion phasing in B-220-250, where elevated temperatures promote NO-to-NOx oxidation pathways, converting 38–42 % of initial NO into N₂O/NO₂ via Zeldovich mechanism extensions [56]. Therefore, under many working conditions, the power and economy of B-220-250 are the best.

4.2. The effect of rotational speed on the engine

Rotating speed, a critical parameter reflecting operational status, exerts multifaceted influences on combustion dynamics and emission characteristics. Building upon the aforementioned investigation of 25 hydrogen/ammonia injection timing configurations, Condition B-220-250 identified as the optimal case demonstrating 71.48 % NO emission reduction and superior thermal efficiency was systematically

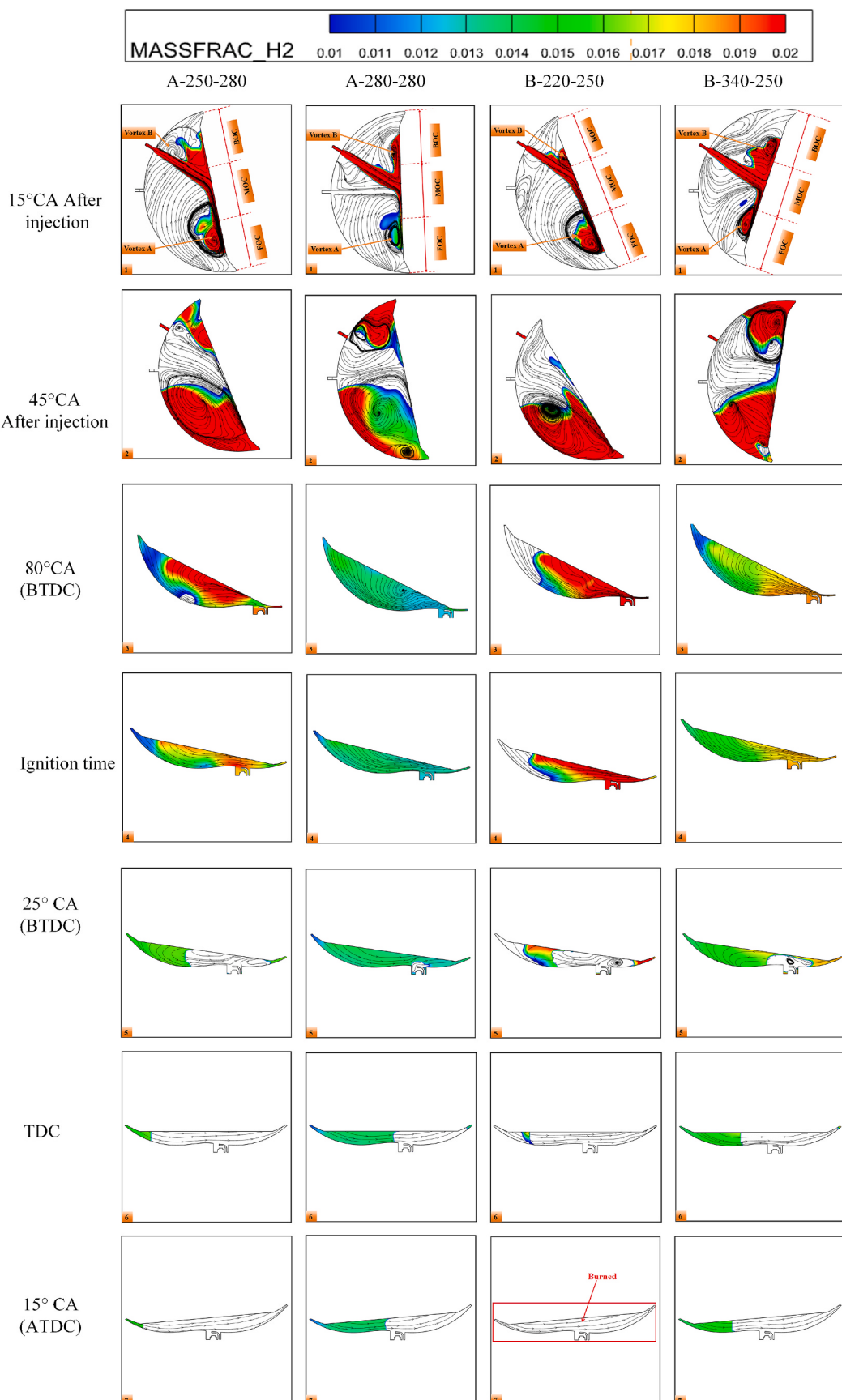


Fig. 8. In-cylinder hydrogen distribution and flow field evolution under varied hydrogen/ammonia injection timings.

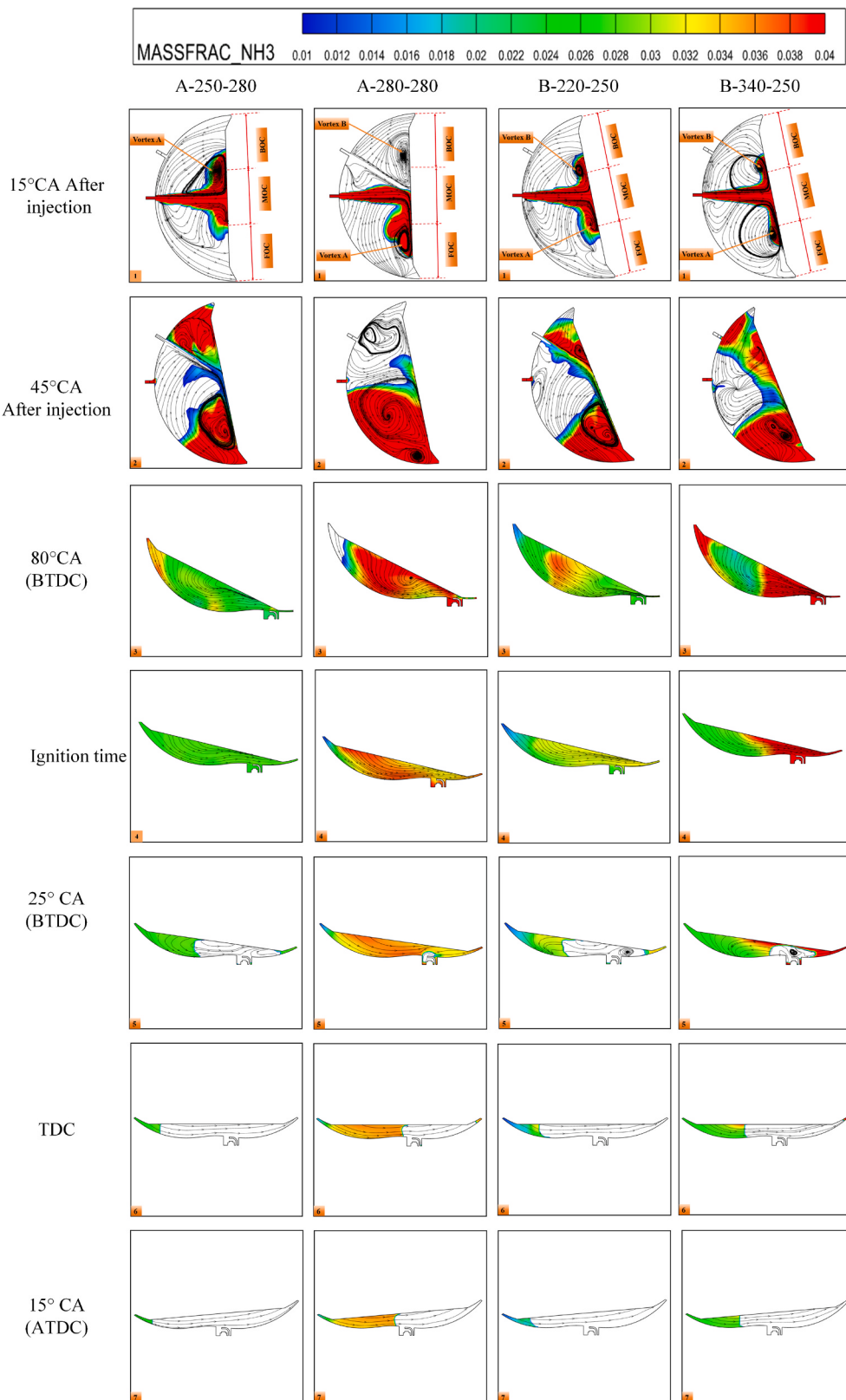


Fig. 9. In-cylinder ammonia distribution and flow field evolution under varied hydrogen/ammonia injection timings.

investigated to evaluate speed-dependent combustion phasing and emission speciation. Detailed operating parameters across tested speed ranges are provided in Table 5.

4.2.1. The effect of the combustion performance

Fig. 14 delineates the in-cylinder pressure and heat release rate characteristics across varying rotating speeds. As shown in Fig. 14(a), the peak in-cylinder pressure initially increases and subsequently decreases within the 1000–3000 r/min speed range. Notably, no ignition

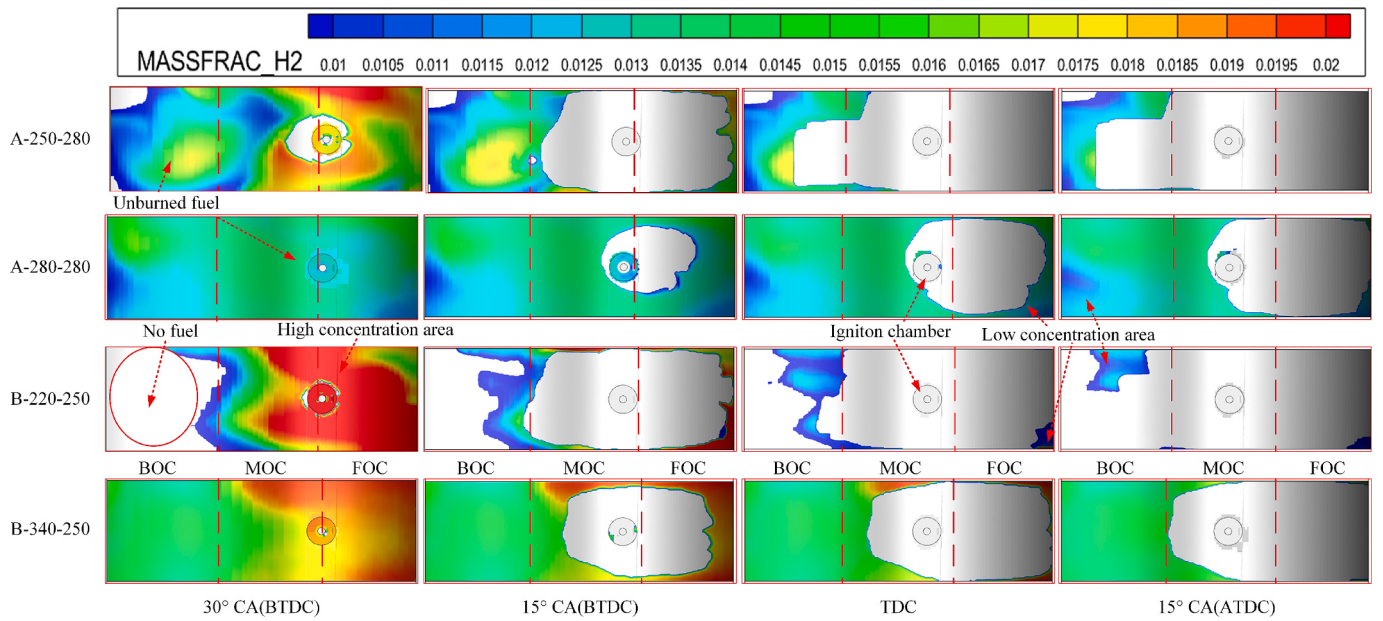


Fig. 10. Unburned hydrogen distribution under varied hydrogen/ammonia injection timings across crank angles.

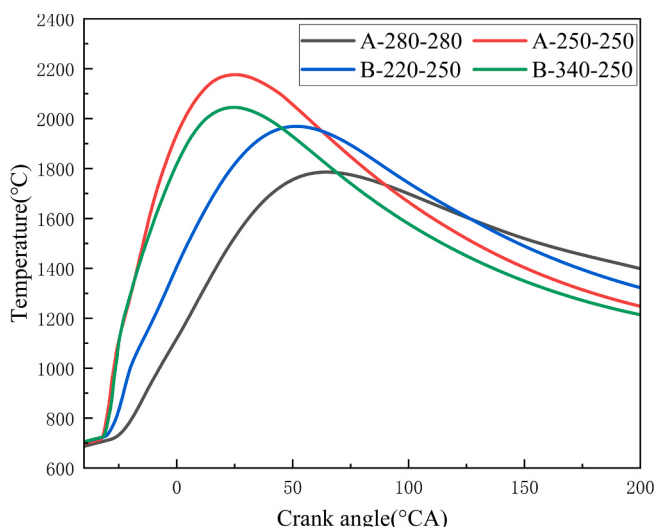


Fig. 11. The temperature profiles under varied hydrogen/ammonia direct injection timings across crank angles.

occurs at 3000 r/min, with detailed failure mechanisms analyzed in Fig. 16. At 1200 r/min and 1400 r/min, peak pressures reach 3.78 MPa and 3.39 MPa, respectively, representing a 11.50 % pressure elevation at the lower speed condition.

Fig. 14 (b) reveals instantaneous heat release rates of 17.41 J/°CA and 10.11 J/°CA at 1200 r/min and 1400 r/min, respectively, corresponding to 72.21 % enhancement in heat release intensity at the optimized speed. The diminished thermal release at elevated speeds stems from two primary mechanisms: (1) Reduced residence time for hydrogen/ammonia mixture preparation near the spark plug, inducing suboptimal fuel stratification; (2) Mismatch between flame propagation velocities (hydrogen: ~2.8 m/s; ammonia: ~0.3 m/s) and rotor tip speeds (exceeding 15 m/s at 3000 r/min), which disrupts flame propagation.

As shown in Fig. 15, the ignition delay, CA50 and combustion duration at different rotating speeds are presented. When the rotating speed is 1200 r/min, the CA90 is 48.84 °CA, which is a 32.78 % reduction in combustion duration compared to that at 1400 r/min. It

was also found that with the increase of rotating speed, CA10 and CA50 gradually increase, while CA90 first decreases and then increases. The main reason is that as the speed of the rotary engine increases, the turbulence intensity of the in-cylinder gas changes. Moderate turbulence can promote combustion, but when the speed is too high, the turbulence may become too chaotic, leading to unstable flame propagation. This turbulence-induced suppression of flame propagation velocity prolongs the combustion process, consequently increasing the required crank angle for achieving specific combustion phases. Furthermore, at high rotational speeds, the ignition system demonstrates reduced capability to consistently initiate air-fuel mixture ignition at optimal timing. The combined effects of extended ignition delay and decelerated combustion rates result in phase-shifted combustion characteristics, manifested as progressive increments in CA10, CA50 and CA90 parameters.

Fig. 16 illustrates the effects of different rotary speeds on indicated work and indicated mean effective pressure (IMEP). It is observed that at a rotary speed of 1400 r/min, the indicated work and IMEP reach their maximum values of 80.77 N·m and 5842830 Pa, respectively. Compared with those at 1000 r/min, the indicated work and IMEP are enhanced by 26.41 %, 20.00 %, respectively. At 1400 r/min, the mixture of hydrogen and ammonia gases can be thoroughly mixed with air. The rotary engine's geometric configuration facilitates optimized gas dynamics, where temporal synchronization of intake, compression, power, and exhaust strokes enables superior air-fuel mixing. This enhanced mixture preparation promotes complete combustion, thereby elevating both indicated work and IMEP. Concurrently, the flame propagation velocity reaches its optimal range at this speed, allowing rapid yet complete combustion within the ideal crank angle window. This efficient energy release mechanism effectively converts chemical energy into enhanced mechanical output.

4.2.2. Effects on fuel distribution and temperature field

As shown in Fig. 17, the distribution of hydrogen and ammonia concentration contours in the cylinder at different rotary speeds at the ignition timing reveals that at speeds of 1000–1400 r/min, H₂ forms distinct high-concentration zones (red regions) in the combustion chamber, which are concentrated in distribution. As the rotary speeds increase to 1600–3000 r/min, these high-concentration zones gradually disperse, indicating that the mixing degree of H₂ changes with increasing rotary speeds. At 1000 r/min, the high-concentration zones of NH₃ are localized. As the rotary speed increases, these high-

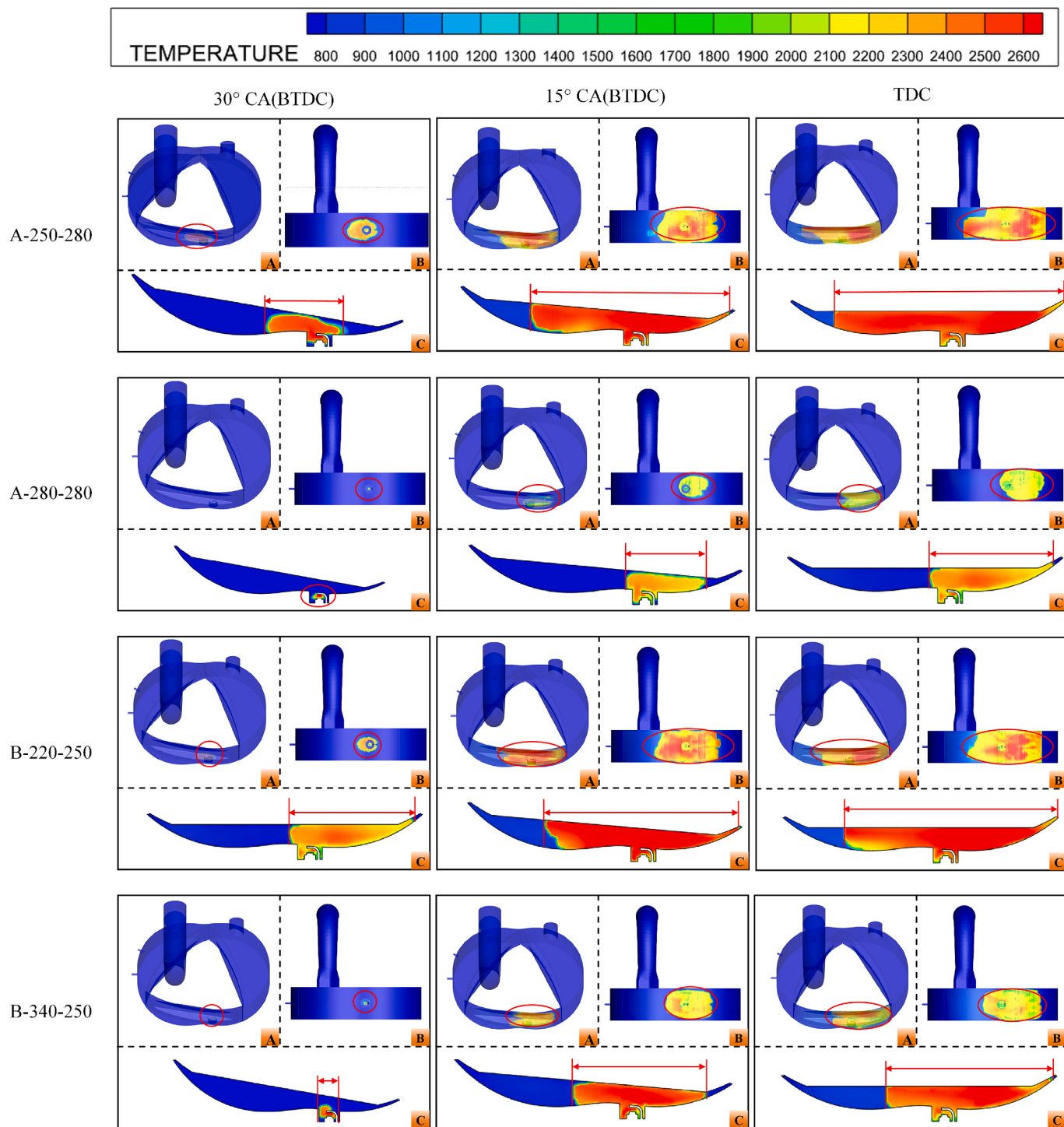


Fig. 12. The temperature field under varied hydrogen/ammonia direct injection timings across crank angles (A: 3D Contour, B: Top Views, C: 2D Front Views).

concentration zones decrease in size, while the low-concentration zones expand, especially at 1800–3000 r/min, where the low-concentration zones become more pronounced. This indicates that the distribution of NH₃ becomes more uniform and the concentration decreases with increasing rotary speeds. At low rotary speeds, the airflow velocity is low, and H₂ and NH₃ have ample time to mix within the combustion chamber.

This leads to the formation of localized high-concentration clusters due to inefficient mixing dominated by molecular diffusion. According to turbulence theory, high rotary speeds enhance the turbulence intensity of the airflow, accelerating the diffusion of components.

Mechanical turbulence dominates the mixing process, shortening the mixing time and promoting the uniform distribution of H₂ and NH₃, thereby dispersing high-concentration regions. From the perspective of reaction kinetics, H₂, being a highly reactive fuel, preferentially participates in reactions in its localized high-concentration zones at low rotary speeds. In contrast, NH₃, with lower reactivity, is mainly distributed according to the flow field. At high rotary speeds, the overall reaction rate increases, altering the dynamic balance between component consumption and diffusion, and further reshaping the concentration distribution characteristics of H₂ and NH₃.

Fig. 18 illustrates the effect of rotary speed on the in-cylinder

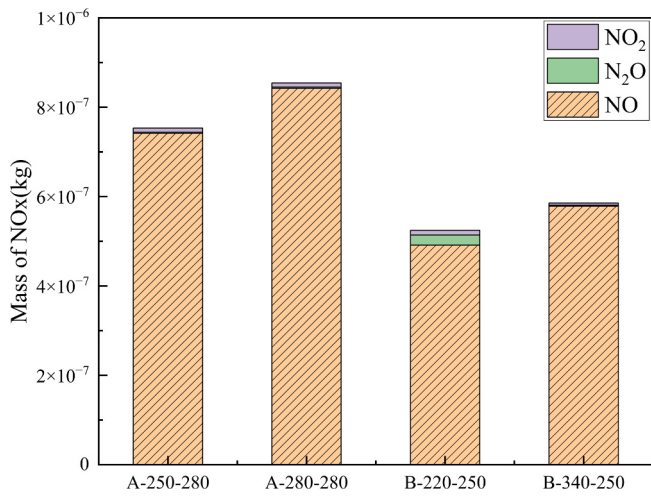


Fig. 13. The influence of different working conditions on emissions.

Table 5
The calculation scheme with different rotating speed.

Case	Speed (r/min)
B-220-250	1000
B-220-250	1200
B-220-250	1400
B-220-250	1600
B-220-250	1800
B-220-250	2000
B-220-250	3000

temperature field under the conditions of hydrogen injection timing at 220 CA (BTDC) and ammonia injection timing at 250 CA (BTDC). From 30 °CA (BTDC) to 15 °CA (BTDC), the low-temperature region contracts, while at TDC, the high-temperature region further expands, occupying a larger area. This indicates that the temperature continuously rises and tends to spread during the combustion process. As the crank angle advances from 30 °CA (BTDC) to TDC, the rotary engine compresses the mixture, causing its temperature to rise during compression. Meanwhile, the combustion reaction intensifies after ignition, releasing a large amount of heat, which leads to the continuous expansion of the high-temperature region in the temperature field. Near TDC, the combustion reaction approaches its peak, releasing the most heat and causing

the high-temperature region to reach its maximum extent. Additionally, the temperature field distribution varies at different rotary speeds. As the rotary speed increases from 1000 r/min to 2000 r/min, at the same crank angle, overall, at 1000–1400 r/min, the high-temperature region expands more significantly and reaches higher temperatures near TDC. However, at 1800–2000 r/min, although the temperature still rises, the expansion rate and extent of the high-temperature region appear to be smaller than those at medium and low speeds under certain crank angles.

At 1000–1400 r/min, the intake duration is relatively longer, allowing the mixture more time to blend and form an appropriate concentration distribution. During compression, the relatively uniform mixture facilitates complete combustion reactions, resulting in a larger high-temperature region near TDC. As the rotary speed increases, the intake duration shortens, and the mixture may not be fully blended, affecting combustion efficiency and limiting the expansion of the high-temperature region under certain crank angles. At 1800–2000 r/min, the gas flow velocity is high and the heat transfer efficiency is relatively higher. Some heat may be more quickly transferred to the cylinder walls and other components, leading to a certain degree of suppression in the

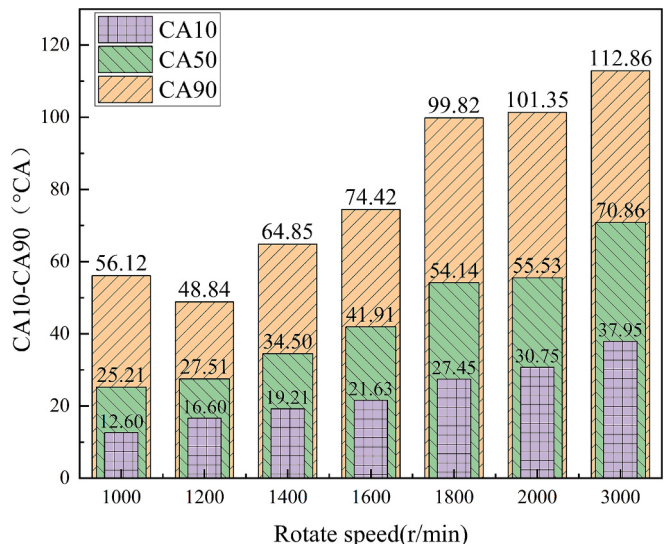


Fig. 15. Ignition delay, CA50, and combustion duration at different rotating speed.

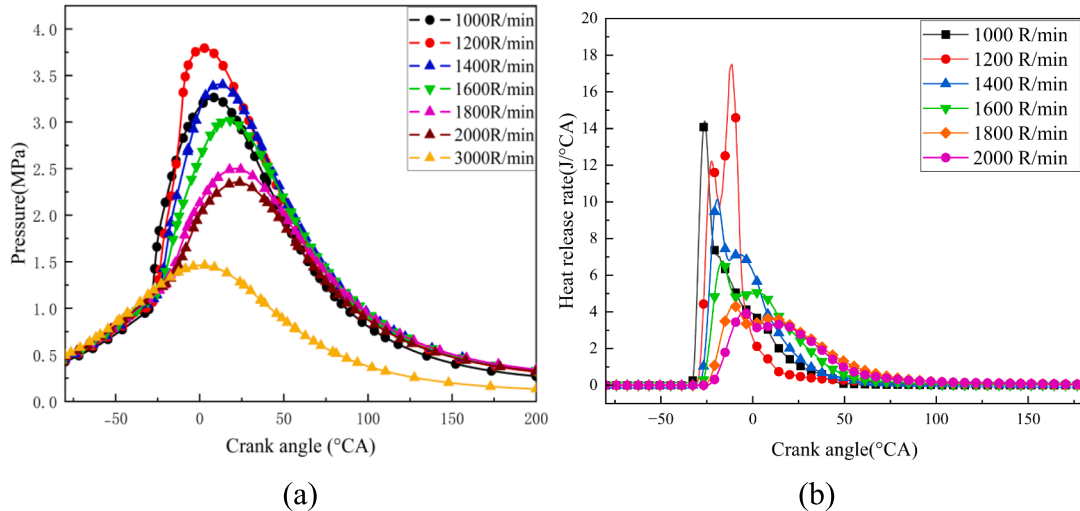


Fig. 14. In-cylinder pressure and heat release rate at different rotating speed.

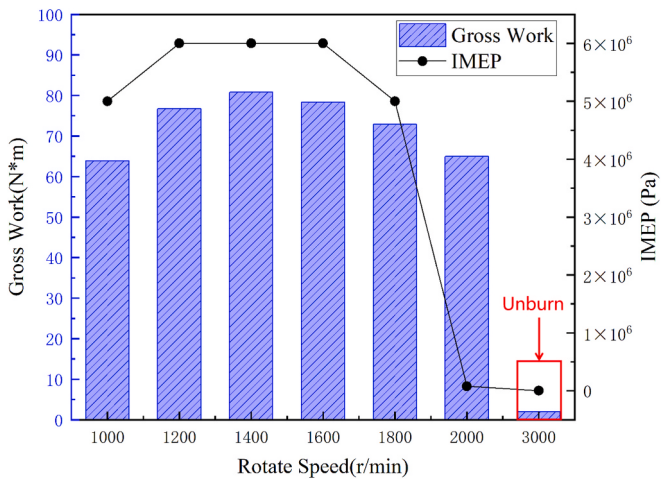


Fig. 16. Indicated Mean Effective Pressure work of the rotary engine at different rotary speeds.

rate of temperature rise and the extent of the high-temperature region in the combustion chamber. Unlike at medium and low speeds, a large high-temperature region is not formed near TDC. As the rotary speed increases, the rotor's movement accelerates and the combustion reaction time is shortened. Chemical reaction kinetics indicates that completing the combustion reaction in a shorter time may not be as thorough as at lower speeds, resulting in differences in the amount of heat released and the extent of the high-temperature region's expansion.

4.3. Effects on emission performance

Fig. 19 shows the effect of different rotary speeds on the formation of NOx within the cylinder. It indicates that the mass of NOx first increases and then decreases with increasing rotary speed. At 1000 r/min, the mass of NOx is 0.96×10^{-7} kg; it reaches a peak of 8.07×10^{-7} kg at 1800 r/min. It decreases to 7.37×10^{-7} kg at 2000 r/min. As shown in Fig. 17, at 1000–1400 r/min, the engine's intake volume is relatively low, resulting in a richer in-cylinder mixture and lower oxygen concentration. NOx formation, particularly thermal NOx, requires the participation of oxygen in the reaction. Low oxygen concentration limits its formation. In contrast, at 1600–2000 r/min, the intake volume is larger and the in-cylinder oxygen concentration is more sufficient, which is conducive to NOx formation.

In summary, considering the comprehensive factors within the combustion chamber of the rotary engine, such as cylinder pressure, heat release rate, effective work and NOx emissions, a rotary speed of 1200–1400 r/min ensures efficient and stable combustion of the fuel with low NOx emissions. At this rotary speed, cylinder pressure, and heat release rate are increased by 11.50 % and 72.21 %, respectively, while NOx emissions are reduced by 17.57 %. The combustion process within this speed range is relatively ideal, with moderate turbulence intensity that facilitates thorough mixing of fuel and air, thereby promoting complete combustion. Additionally, the moderate rotary speed is conducive to precise ignition control, ensuring ignition at the optimal moment and further enhancing combustion efficiency. Moreover, the combustion process within this speed range effectively controls the combustion temperature, preventing the excessive formation of NOx due to high temperatures, thus achieving the goal of low emissions.

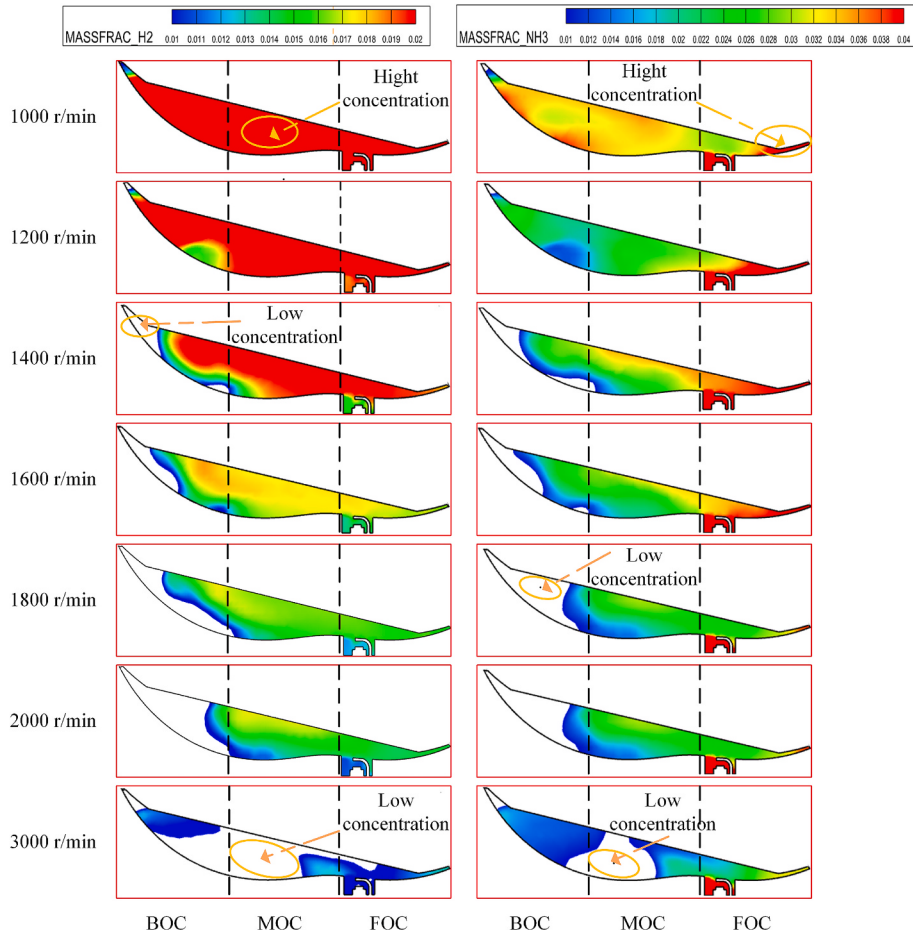


Fig. 17. In-cylinder fuel distribution at different rotary speeds at ignition timing.

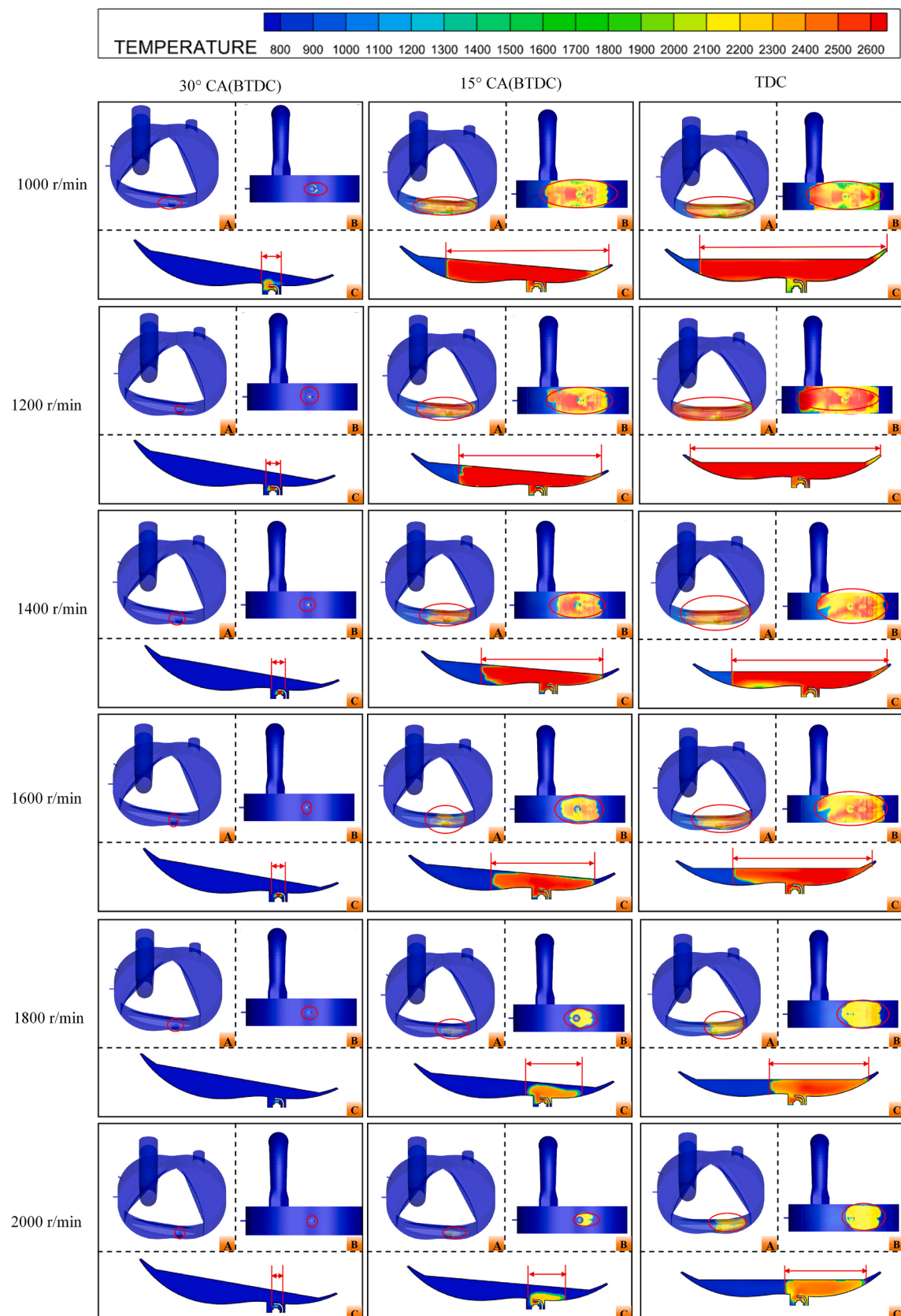


Fig. 18. Temperature distribution at different rotating speed (A: 3D Contour, B: Top Views, C: 2D Front Views).

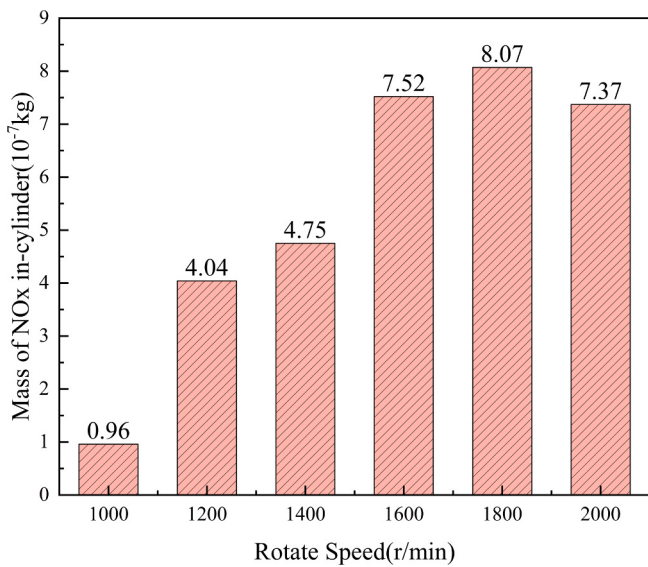


Fig. 19. Different rotating speeds cause different levels of emissions.

Therefore, a rotary speed of 1200–1400 r/min is an optimized choice for achieving efficient combustion and environmentally friendly emissions.

5. Conclusion and perspective

A 3D dual direct-injection model investigates how hydrogen/ammonia injection timings and rotational speeds affect mixture formation, flame propagation, and NOx emissions. Results confirm 100 % stable, complete combustion with hydrogen-ammonia dual fuel, supporting “green ammonia-hydrogen” zero-carbon applications in distributed energy and advancing energy structure decarbonization. Compared to conventional gas engines, this scheme retains high power density while achieving near-zero carbon emissions, enabling power upgrades in aviation, vehicle-mounted, and other sectors. The main conclusions are as follows:

Regarding the dual direct injection of hydrogen and ammonia at different timings in the cylinder, it was observed that delaying the injection of both fuels significantly increases the peak in-cylinder pressure by 10.10 % and shortens the combustion duration by 10.01 % compared to the C-280-220 operating condition. Notably, the injection combinations of A-250-280 and B-220-250 have the most significant impact on cylinder pressure and combustion duration. This indicates that under appropriate injection timings, the hydrogen and ammonia mixture can burn more efficiently, thereby improving combustion efficiency and reducing energy losses during the combustion process.

As hydrogen injection is delayed to 220-250 °CA BTDC, the formation of stratified mixtures within the cylinder is promoted. This enhances combustion efficiency and reduces NOx emissions by increasing the in-cylinder temperature and optimizing mixture stratification. Concurrently, direct injection of ammonia at 250-280 °CA BTDC results in a more uniform mixture distribution, thereby improving ammonia combustion efficiency and reducing unburned ammonia emissions. The optimal combustion and emission performance are achieved with a fuel distribution that forms a hydrogen core surrounded by an ammonia layer. These findings underscore the importance of optimizing fuel injection timings to enhance combustion performance and reduce pollutant emissions.

The effect of different rotary speeds on combustion is mainly manifested as follows: within the rotary speed range of 1000–2000 r/min, cylinder pressure, effective work, and heat release rate first increase and then decrease. Considering the comprehensive factors

within the combustion chamber of the rotary engine, such as cylinder pressure, heat dissipation rate, effective work and NOx emissions, a rotary speed of 1200–1400 r/min ensures low NOx emissions and efficient, stable combustion of the fuel. At this rotary speed, cylinder pressure, heat release rate, and effective work are increased by 11.50 %, 72.21 %, and 26.41 % respectively, while NOx emissions are reduced by 17.57 %.

The simulation results indicate that when the injection timings of hydrogen and ammonia are set at A-250-280 and B-220-250, respectively, the combustion state is optimal. Delayed hydrogen injection helps to form stratified mixtures, thereby enhancing combustion efficiency. Under the rotary speed range of 1200–1400 r/min, this combination of injection timings significantly optimizes the in-cylinder combustion process. Within this speed range, the optimized combustion process not only improves combustion efficiency but also effectively reduces NOx emissions. Therefore, the rotary speed range of 1200–1400 r/min, combined with optimized injection timings, is an ideal choice for achieving efficient and clean combustion.

In contrast to conventional gasoline combustion, in which delayed injection usually results in a reduction in peak pressure due to diminished premixed combustion, hybrid direct injection of hydrogen and ammonia typically produces a higher peak pressure. Because hydrogen has a rapid reactivity, it counteracts the retarded injection timing by increasing the intensity of combustion.

CRediT authorship contribution statement

Weng Fu: Writing – original draft, Investigation, Data curation. **Jianfeng Pan:** Writing – review & editing, Supervision. **Baowei Fan:** Resources, Methodology, Conceptualization. **Yi Zhang:** Resources, Investigation, Conceptualization. **Xia Shao:** Investigation, Conceptualization. **Muhammad Nauman:** Writing – review & editing. **Wenming Yang:** Resources, Conceptualization.

Declaration of competing interest

The authors declare that they have no known competing financial interests or personal relationships that could have appeared to influence the work reported in this paper.

Acknowledgments

This work was supported by the National Natural Science Foundation of China (Grant No. 52276117; No. 51976083), Qing Lan Project, a Project funded by China Postdoctoral Science Foundation (No. 2023T160550), Natural Science Foundation of Jiangsu Province (BK20230535).

Data availability

No data was used for the research described in the article.

References

- [1] Singh P, Paparao J, Singh P, Kumbhakarna N, Kumar S. A review of recent advances in hydrogen fueled Wankel engines for clean energy transition and sustainable mobility. Fuel 2025;387:134334. <https://doi.org/10.1016/j.fuel.2025.134334>.
- [2] Jafar U, Nuhu U, Khan WU, Hossain MM. A review on green ammonia as a potential CO₂ free fuel. Int J Hydrom Energy 2024;71:857–76. <https://doi.org/10.1016/j.ijhydene.2024.05.128>.
- [3] Kilkış Ş, Krajačić G, Duić N, Rosen MA, Ahmad A-N. Sustainable development of energy, water and environment systems as a key opportunity for decarbonisation. Energy Convers Manag 2024;320:118953. <https://doi.org/10.1016/j.enconman.2024.118953>.
- [4] Alagumalai A. Internal combustion engines: progress and prospects. Renew Sustain Energy Rev 2014;38:561–71. <https://doi.org/10.1016/j.rser.2014.06.014>.

- [5] Algayyim SJM, Saleh K, Wandel AP, Fattah IMR, Yusaf T, Alrazen HA. Influence of natural gas and hydrogen properties on internal combustion engine performance, combustion, and emissions: a review. *Fuel* 2024;362:130844. <https://doi.org/10.1016/j.fuel.2023.130844>.
- [6] Mohan B, Yang W, Chou S kiang. Fuel injection strategies for performance improvement and emissions reduction in compression ignition engines—a review. *Renew Sustain Energy Rev* 2013; 28:664–76. doi: 10.1016/j.rser.2013.08.051.
- [7] Sadiq GA, Al-Dadah R, Mahmoud S. Development of rotary Wankel devices for hybrid automotive applications. *Energy Convers Manag* 2019;202:112159. <https://doi.org/10.1016/j.enconman.2019.112159>.
- [8] Warren S, Yang DCH. Design of rotary engines from the apex seal profile (abbr.: Rotary engine design by apex seal). *Mech Mach Theory* 2013;64. <https://doi.org/10.1016/j.mechmachtheory.2013.01.015>.
- [9] Zambalov SD, Yakovlev IA, Maznay AS. Effect of multiple fuel injection strategies on mixture formation and combustion in a hydrogen-fueled rotary range extender for battery electric vehicles. *Energy Convers Manag* 2020;220:113097. <https://doi.org/10.1016/j.enconman.2020.113097>.
- [10] Awais M, Li W, Hussain S, Cheema MJM, Li W, Song R, et al. Comparative evaluation of land surface temperature images from unmanned aerial vehicle and satellite observation for agricultural areas using in situ data. *Agriculture* 2022;12: 184. <https://doi.org/10.3390/agriculture12020184>.
- [11] Li H, Chen L, Zhang Z. A study on the utilization rate and influencing factors of small agricultural machinery: evidence from 10 hilly and mountainous Provinces in China. *Agriculture* 2022;12:51. <https://doi.org/10.3390/agriculture13010051>.
- [12] Shi Q, Liu D, Mao H, Shen B, Li M. Wind-induced response of rice under the action of the downwash flow field of a multi-rotor UAV. *Biosyst Eng* 2021;203:60–9. <https://doi.org/10.1016/j.biosystemseng.2020.12.012>.
- [13] Zhang S, Xue X, Chen C, Sun Z, Sun T, 1. Nanjing Research Institute for Agricultural Mechanization, Ministry of Agriculture and Rural Affairs, Nanjing 210014, China, et al. Development of a low-cost quadrotor UAV based on ADRC for agricultural remote sensing. *Int J Agric Biol Eng* 2019; 12:82–7. doi: 10.25165/j.ijabe.20191204.4641.
- [14] Carvalho FS, Lacava PT, Rufino CH, Travieso Pedroso D, Blanco Machin E, H. M. Araújo F, et al. Mixtures of heavy fuel oil and green hydrogen in combustion equipment: Energy analysis, emission estimates, and economic prospects. *Energy Convers Manag* 2023; 277:116629. doi: 10.1016/j.enconman.2022.116629.
- [15] Tutak W, Jamrozik A, Grab-Rogaliński K, Pyrc M. Effects of ammonia energy fraction on combustion stability and emissions characteristics of naturally aspirated industrial dual-fuel diesel engine. *Energy Convers Manag* 2024;314:118698. <https://doi.org/10.1016/j.enconman.2024.118698>.
- [16] Amrouche F, Erickson PA, Varnhagen S, Park JW. An experimental study of a hydrogen-enriched ethanol fueled wankel rotary engine at ultra lean and full load conditions. *Energy Convers Manag* 2016;123:174–84. <https://doi.org/10.1016/j.enconman.2016.06.034>.
- [17] Shahir SA, Masjuki HH, Kalam MA, Imran A, Fattah IMR, Sanjid A. Feasibility of diesel-biodiesel-ethanol/bioethanol blend as existing CI engine fuel: an assessment of properties, material compatibility, safety and combustion. *Renew Sustain Energy Rev* 2014;32:379–95. <https://doi.org/10.1016/j.rser.2014.01.029>.
- [18] Cheng X, Li Y, Xu Y, Liu Y, Wang B. Study of effects of ammonia addition on soot formation characteristics in n-heptane co-flow laminar diffusion flames. *Combust Flame* 2022;235:111683. <https://doi.org/10.1016/j.combustflame.2021.111683>.
- [19] Tian Z, Li Y, Zhang L, Glarborg P, Qi F. An experimental and kinetic modeling study of premixed NH₃/CH₄/O₂/Ar flames at low pressure. *Combust Flame* 2009; 156:1413–26. <https://doi.org/10.1016/j.combustflame.2009.03.005>.
- [20] Wu Y, Mei J, Cai T, Wang W, Zhu H, Sun T, et al. Reducing the NO_x emissions during NH₃ oxidation with Nickel modified Fe₂O₃-a promising cost-effective and environmentally friendly catalyst for NH₃ combustion. *Combust Flame* 2022;237: 111845. <https://doi.org/10.1016/j.combustflame.2021.111845>.
- [21] Yu L, Zhou W, Feng Y, Wang W, Zhu J, Qian Y, et al. The effect of ammonia addition on the low-temperature autoignition of n-heptane: an experimental and modeling study. *Combust Flame* 2020;217:4–11. <https://doi.org/10.1016/j.combustflame.2020.03.019>.
- [22] Liu L, Wu Y, Wang Y. Numerical investigation on the combustion and emission characteristics of ammonia in a low-speed two-stroke marine engine. *Fuel* 2022; 314:122727. <https://doi.org/10.1016/j.fuel.2021.122727>.
- [23] Ryu K, Zacharakis-Jutz GE, Kong S-C. Effects of gaseous ammonia direct injection on performance characteristics of a spark-ignition engine. *Appl Energy* 2014;116: 206–15. <https://doi.org/10.1016/j.apenergy.2013.11.067>.
- [24] Oh S, Park C, Kim S, Kim Y, Choi Y, Kim C. Natural gas-ammonia dual-fuel combustion in spark-ignited engine with various air-fuel ratios and split ratios of ammonia under part load condition. *Fuel* 2021;290:120095. <https://doi.org/10.1016/j.fuel.2020.120095>.
- [25] Zhu T, Yan X, Gao Z, Qiu Y, Zhu L, Huang Z. Combustion and emission characteristics of ammonia-hydrogen fueled SI engine with high compression ratio. *Int J Hydrog Energy* 2024;62:579–90. <https://doi.org/10.1016/j.ijhydene.2024.03.035>.
- [26] Nauman M, Pan J, Lu Q, Zhang Y, Liu C, Li F, et al. Analyzing the combustion characteristics of premixed methane-oxygen with different hydrogen addition ratios in a catalytic micro-combustor. *J Energy Inst* 2024;114:101655. <https://doi.org/10.1016/j.joei.2024.101655>.
- [27] Yang J, Ji C, Wang S, Wang D, Ma Z, Ma L. A comparative study of mixture formation and combustion processes in a gasoline wankel rotary engine with hydrogen port and direct injection enrichment. *Energy Convers Manag* 2018;168: 21–31. <https://doi.org/10.1016/j.enconman.2018.04.105>.
- [28] Taskiran OO, Calik AT, Akin KO. Comparison of flow field and combustion in single and double side ported rotary engine. *Fuel* 2019;254:115651. <https://doi.org/10.1016/j.fuel.2019.115651>.
- [29] Yang J, Ji C, Wang S, Zhang Z, Wang D, Ma Z. Numerical investigation of the effects of hydrogen enrichment on combustion and emissions formation processes in a gasoline rotary engine. *Energy Convers Manag* 2017;151:136–46. <https://doi.org/10.1016/j.enconman.2017.08.070>.
- [30] Picard M, Tian T, Nishino T. Predicting gas leakage in the rotary engine—part II: Side seals and summary. *J Eng Gas Turbines Power* 2016;138:062504. <https://doi.org/10.1115/1.4031874>.
- [31] Picard M, Tian T, Nishino T. Predicting gas leakage in the rotary engine—part I: Apex and corner seals. *J Eng Gas Turbines Power* 2016;138:062503. <https://doi.org/10.1115/1.4031873>.
- [32] Nauman M, Pan J, Wang Y, Li F, Oluwaleke Ojo A, Raza A. A review of recent advancements in micro combustion techniques to enhance flame stability and fuel residence time. *Int J Hydrog Energy* 2024;49:1165–93. <https://doi.org/10.1016/j.ijhydene.2023.09.050>.
- [33] Ozcanli M, Bas O, Akar MA, Yildizhan S, Serin H. Recent studies on hydrogen usage in Wankel SI engine. *Int J Hydrog Energy* 2018;43:18037–45. <https://doi.org/10.1016/j.ijhydene.2018.01.202>.
- [34] Meng H, Ji C, Wang S, Wang D, Yang J. Optimizing the idle performance of an n-butanol fueled Wankel rotary engine by hydrogen addition. *Fuel* 2021;288: 119614. <https://doi.org/10.1016/j.fuel.2020.119614>.
- [35] Hong C, Xu S, Zhao S, Zhang H, Su F, Wang S, et al. Analysis of ammonia as a combustion inhibitor for combustion knock and power expansion in a DI hydrogen engine. *Fuel* 2024;375:132481. <https://doi.org/10.1016/j.fuel.2024.132481>.
- [36] Hong C, Xin G, Xu S, Cai J, Su F, Wang S, et al. An experimental study of knock in a DI hydrogen engine: the synergistic effects of the deep miller cycle and oxygen-enriched atmosphere. *Energy Convers Manag* 2024;306:118269. <https://doi.org/10.1016/j.enconman.2024.118269>.
- [37] Huang Y, Huang S, Huang R, Hong G. Spray and evaporation characteristics of ethanol and gasoline direct injection in non-evaporating, transition and flash-boiling conditions. *Energy Convers Manag* 2016;108:68–77. <https://doi.org/10.1016/j.enconman.2015.10.081>.
- [38] Kang R, Zhou L, Hua J, Feng D, Wei H, Chen R. Experimental investigation on combustion characteristics in dual-fuel dual-injection engine. *Energy Convers Manag* 2019;181:15–25. <https://doi.org/10.1016/j.enconman.2018.11.057>.
- [39] Li P, Pan J, Fan B, Quaye EK, Zhang Y, Weng J, et al. The effect of dual injection strategy on fuel distribution and combustion characteristics in ammonia/hydrogen rotary engines. *Energy* 2025;332:137119. <https://doi.org/10.1016/j.energy.2025.137119>.
- [40] Rameez PV, Mohamed IM. Estimation of assorted injection schedules on hydrogen-diesel dual fuel and reactivity controlled compression ignition modes in a medium duty automotive engine. *Fuel* 2024;359:130435. <https://doi.org/10.1016/j.fuel.2023.130435>.
- [41] Yin X, Yan Y, Ren X, Yu L, Duan H, Hu E, et al. Effects of methanol energy substitution ratio and diesel injection timing on a methanol/diesel dual-fuel direct injection engine. *Fuel* 2025;382:133773. <https://doi.org/10.1016/j.fuel.2024.133773>.
- [42] Wang Z, Yang C, Zhang F, Cheng X. Effects of diesel injector nozzle angle and split diesel injection strategy on combustion and emission characteristics of an ammonia/diesel dual-fuel engine. *Energy* 2024;307:132686. <https://doi.org/10.1016/j.energy.2024.132686>.
- [43] Wang W, Tang C, Huang Z. Diesel-natural gas dual fuel injection strategy effects on engine ignition delay and cylinder pressure evolution. *Case Stud Therm Eng* 2024; 53:103795. <https://doi.org/10.1016/j.csite.2023.103795>.
- [44] Feng S, Zhang S, Zhang H, Shi J. Effect of nozzle geometry on combustion of a diesel-methanol dual-fuel direct injection engine. *Fuel* 2024;357:129734. <https://doi.org/10.1016/j.fuel.2023.129734>.
- [45] Fan B, Pan J, Liu Y, Zhu Y, Pan Z, Chen W, et al. Effect of hydrogen injection strategies on mixture formation and combustion process in a hydrogen direct injection plus natural gas port injection rotary engine. *Energy Convers Manag* 2018;160:150–64. <https://doi.org/10.1016/j.enconman.2018.01.034>.
- [46] Ji C, Chang K, Wang S, Yang J, Wang D, Meng H, et al. Effect of injection strategy on the mixture formation and combustion process in a gasoline direct injection rotary engine. *Fuel* 2021;304:121428. <https://doi.org/10.1016/j.fuel.2021.121428>.
- [47] Lu Y, Pan J, Fan B, Otchere P, Chen W, Cheng B. Research on the application of aviation kerosene in a direct injection rotary engine-Part 1: fundamental spray characteristics and optimized injection strategies. *Energy Convers Manag* 2019; 195:519–32. <https://doi.org/10.1016/j.enconman.2019.05.042>.
- [48] Lu Y, Pan J, Fan B, Otchere P, Chen W, Cheng B. Research on the application of aviation kerosene in a direct injection rotary engine – Part 2: Spray combustion characteristics and combustion process under optimized injection strategies. *Energy Convers Manag* 2020;203:112217. <https://doi.org/10.1016/j.enconman.2019.112217>.
- [49] Fan B, Zeng Y, Pan J, Fang J, Salami HA, Wang Y. Numerical study of injection strategy on the combustion process in a peripheral ported rotary engine fueled with natural gas/hydrogen blends under the action of apex seal leakage. *Energy* 2022; 242:122532. <https://doi.org/10.1016/j.energy.2021.122532>.
- [50] Gotama GJ, Hayakawa A, Okafor EC, Kanoshima R, Hayashi M, Kudo T, et al. Measurement of the laminar burning velocity and kinetics study of the importance of the hydrogen recovery mechanism of ammonia/hydrogen/air premixed flames. *Combust Flame* 2022;236:111753. <https://doi.org/10.1016/j.combustflame.2021.111753>.

- [51] Fan B, Wu X, Pan J, Qi X, Fang J, Lu Q, et al. Research on the structure of pre-chamber and jet orifice of a turbulent jet ignition rotary engine fueled with methanol/gasoline blends. *Appl Therm Eng* 2023;229:120588. <https://doi.org/10.1016/j.applthermaleng.2023.120588>.
- [52] Yang Z, Du Y, Jia G, Gao X, Fang Z, He G, et al. Clean combustion of a hydrogen-doped elliptical rotary engine based on turbulent jet ignition: Synergistic enhancement of thermodynamic and emission performance via flow field coupling. *Energy Convers Manag* 2025;343:120154. <https://doi.org/10.1016/j.enconman.2025.120154>.
- [53] Grimaldi CN, Millo F. Internal Combustion Engine (ICE) Fundamentals. In: Yan J, editor. Handb. Clean Energy Syst. 1st ed., Wiley; 2015, p. 1–32. doi: 10.1002/978118991978.hces077.
- [54] Rajasegar R, Niki Y, Garcia-Oliver JM, Li Z, Musculus MPB. Fundamental insights on ignition and combustion of natural gas in an active fueled pre-chamber spark-ignition system. *Combust Flame* 2021;232:111561. <https://doi.org/10.1016/j.combustflame.2021.111561>.
- [55] Ji C, Li H, Yang J, Meng H. Numerical investigation on the effect of ignition timing on a low-temperature hydrogen-fueled wankel rotary engine with passive pre-chamber ignition. *Energy* 2024;313:133686. <https://doi.org/10.1016/j.energy.2024.133686>.
- [56] Deng K, He A, Liu Z, Ye S, Lin W, Kang W, et al. Resolving NO_x formation of ammonia-hydrogen flame utilizing PLIF technique collaborated with flame structures and chemical kinetics analysis. *Appl Therm Eng* 2025;259:124842. <https://doi.org/10.1016/j.applthermaleng.2024.124842>.